

1 **Genome-Wide CRISPR-Cas9 Screening Identifies a Synergy between Hypomethylating
2 Agents and SUMOylation Blockade in MDS/AML.**

3
4 Peter Truong¹, Sylvie Shen², Swapna Joshi², Md Imtiazul Islam², Ling Zhong³, Mark J.
5 Raftery³, Ali Afrasiabi⁴, Hamid Alinejad-Rokny^{4,5,6}, Mary Nguyen², Xiaoheng Zou², Golam
6 Sarower Bhuyan², Chowdhury H. Sarowar², Elaheh S. Ghodousi¹, Olivia Stonehouse², Sara
7 Mohamed^{1,7,11}, Cara E. Toscan^{1,7,11}, Patrick Connerty^{1,7,11}, Purvi M. Kakadia⁸, Stefan K.
8 Bohlander⁸, Katharine A. Michie⁹, Jonas Larsson¹⁰, Richard B. Lock^{1,7,11}, Carl R.
9 Walkley^{12,13}, Julie A. I. Thoms², Christopher J. Jolly^{2*}, and John E. Pimanda^{1,2,14*}

10
11
12 ¹*School of Clinical Medicine, UNSW Sydney, Sydney, Australia*

13 ²*School of Biomedical Sciences, UNSW Sydney, Sydney, Australia*

14 ³*Bioanalytical Mass Spectrometry Facility, Mark Wainwright Analytical Centre, UNSW
15 Sydney, Sydney, Australia*

16 ⁴*BioMedical Machine Learning Lab, Graduate School of Biomedical Engineering, UNSW
17 Sydney, Sydney, Australia*

18 ⁵*UNSW Data Science Hub, UNSW Sydney, Sydney, Australia*

19 ⁶*Health Data Analytics Program, AI-Enabled Processes Research Centre, Macquarie
20 University, Sydney, Australia*

21 ⁷*Children's Cancer Institute, UNSW Sydney, Sydney, Australia*

22 ⁸*Leukaemia and Blood Cancer Research Unit, Department of Molecular Medicine and
23 Pathology, University of Auckland, Auckland, New Zealand*

24 ⁹*Structural Biology Facility, Mark Wainwright Analytical Centre, UNSW Sydney, Sydney,
25 Australia*

26 ¹⁰*Division of Molecular Medicine and Gene Therapy, Lund Stem Cell Centre, Lund
27 University, Lund, Sweden*

28 ¹¹*University of New South Wales Centre for Childhood Cancer Research, UNSW Sydney,
29 Sydney, Australia*

30 ¹²*St Vincent's Institute of Medical Research, University of Melbourne, Melbourne, Australia*

31 ¹³*Department of Medicine, University of Melbourne, Melbourne, Australia*

32 ¹⁴*Haematology Department, Prince of Wales Hospital, Sydney, Australia*

33

34 *Senior authors

35

36 Correspondence; Dr Christopher Jolly (c.jolly@unsw.edu.au), Dr John Pimanda
37 (jpimanda@unsw.edu.au)

38

39

40

1 **ABSTRACT**

2 Hypomethylating agents (HMAs) are frontline therapies effective at altering the natural
3 course of Myelodysplastic Neoplasms (MDS) and Acute Myeloid Leukemia (AML).
4 However, acquired resistance and treatment failure are hallmarks of HMA therapy. To
5 address this clinical need, we performed a genome-wide CRISPR-Cas9 screen in a human
6 MDS-derived cell line, MDS-L, and identified TOPORS as a highly ranked loss-of-function
7 target that synergizes with HMAs, reducing leukemic burden and improving survival in
8 xenograft models. We demonstrate that the depletion of TOPORS mediates sensitivity to
9 HMAs by predisposing leukemic blasts to an impaired DNA damage response (DDR)
10 accompanied by an accumulation of SUMOylated DNMT1 in HMA-treated TOPORS-
11 depleted cells. Importantly, the combination of HMAs with targeting of TOPORS did not
12 functionally impair healthy hematopoiesis. While inhibitors of TOPORS are currently
13 unavailable, we show that inhibition of protein SUMOylation (upstream of TOPORS
14 functions) with TAK-981 partially phenocopies HMA-sensitivity and DDR impairment.
15 Overall, our data suggest that the combination of HMAs with the inhibition of SUMOylation
16 or TOPORS demonstrates a favourable therapeutic index and is a rational treatment
17 framework for High-Risk MDS (HR-MDS) or AML.

18

19

1 INTRODUCTION

2

3 The cytidine nucleoside analogues Azacitidine (AZA) and Decitabine (DAC) are effective
4 frontline treatments for MDS which promote hematologic recovery and delay transformation
5 to AML¹⁻⁴. Despite their clinical benefit, HMA therapy is limited by transient efficacy as
6 underscored by the high frequency of acquired resistance to recurrent HMA exposure² and
7 disease relapse. Emerging evidence suggests multiple mechanisms of HMA resistance;
8 namely, adaptations of metabolic processes involved in activating HMAs⁵, cell cycle
9 quiescence⁶, disequilibrium between pro- and anti-apoptotic proteins⁷, upregulation of
10 immune checkpoint signalling axes⁸, and re-expression of oncogenes⁹. Allogeneic bone
11 marrow transplants, the only potential curative approach, are feasible for approximately 8%
12 of MDS patients due to their typical frailty¹⁰. Current treatment options for non-responding
13 patients are limited to enrolment into clinical trials or provision of supportive care.

14

15 Strategies to develop combinatorial treatments to overcome acquired drug resistance
16 and tumor heterogeneity have been effective across various cancer types¹¹. In MDS and
17 AML, combining the BCL-2 inhibitor Venetoclax (VEN) with AZA is effective in
18 eradicating malignant leukemic stem cells compared to monotherapy¹². However, the
19 associated extreme rates of febrile neutropenia are of high concern^{13,14}. Combining anti-
20 CD47 (magrolimab) with AZA has also been explored. Preliminary clinical data suggested
21 promising survival benefits, especially in *TP53*-mutated subsets¹⁵, but Phase 3 ENHANCE
22 studies combining magrolimab with AZA (NCT04313881) in HR-MDS, and magrolimab
23 with VEN and AZA in AML (NCT05079230) were discontinued due to futility and increased
24 mortality compared with AZA or AZA and VEN, respectively.

25

1 Current models of drug mode-of-action for HMAs include rewiring of the epigenome
2 to promote the re-expression of silenced tumor suppressor and cellular differentiation
3 genes¹⁶, the induction of endogenous retroviral elements leading to inflammatory viral
4 mimicry responses^{17,18}, and cytotoxicity through the formation of genotoxic covalent
5 DNMT1-DNA adducts¹⁹. To rationally identify secondary agents for combinatorial therapy,
6 the epistatic genetic interactions that define drug response for the anchoring agent need to be
7 systematically mapped. Genome-wide screening approaches can identify synthetic lethal
8 relationships in an unbiased manner without requiring prior knowledge of drug mechanism.
9 Although genome-wide CRISPR-Cas9 screens^{20,21} and targeted RNAi screens to identify
10 resistance and synthetic lethal HMA-gene relationships²² have been performed, a genome-
11 wide CRISPR-Cas9 dropout approach to identify genetic vulnerabilities in MDS cells to low
12 dose HMA therapy has not yet been reported.

13

14 We performed a genome-wide loss-of-function CRISPR-Cas9 dropout screen in *TP53*
15 mutant MDS-L cells in the presence of low-dose AZA and identified the E3-ligase TOPORS
16 as a top sensitization target. In the absence of an available TOPORS inhibitor, we provide
17 genetic proof of concept that targeting TOPORS confers hypersensitivity to HMAs by
18 delaying the clearance of SUMOylated DNMT1 from HMA-treated cells, predisposing
19 leukemia cells to apoptosis. Importantly, this strategy did not impair healthy hematopoiesis.
20 As a surrogate for directly targeting TOPORS, we show that inhibition of SUMOylation
21 using TAK-981 is synergistic with HMAs and phenocopies the DDR impairment observed in
22 *TOPORS*-edited MDS cells without disrupting healthy hematopoietic stem and progenitor
23 cells (HSPC) function. Our work reveals a unique therapeutic approach to enhance HMA
24 response through modulating SUMOylation-dependent DDR, and more broadly, provides a
25 framework for development of effective HMA combinatorial therapies.

1 **RESULTS**

2

3 ***Genome-wide CRISPR-Cas9 dropout screening identifies novel genetic determinants of***
4 ***AZA sensitivity.***

5 MDS-L was selected for genome-wide CRISPR-Cas9 dropout screen as it is the only MDS
6 cell line that faithfully recapitulates MDS pathogenicity *in vivo*²³ and harbors a genetic
7 profile reflective of HR-MDS (del5q, *TP53*^{-/-}, Type II myeloid driver mutations²⁴, Table S1).
8 We chose 0.3μM AZA for dropout screening because compared to higher concentrations it
9 mediated anti-proliferative rather than direct lethality, while maintaining robust levels of
10 demethylation (Fig. S1A). Cas9-expressing MDS-L cells were transduced with the Brunello
11 sgRNA library²⁵ and treated with AZA or vehicle for 12 cellular divisions in the AZA-treated
12 arm (18 divisions in the vehicle-treated arm, Fig. S1B) to ensure robust depletion or
13 enrichment of sgRNAs (Fig. 1A). The quality of the CRISPR-Cas9 screening libraries and
14 the frequency of individual sgRNAs in the two treatment arms were quantified using the
15 MAGeCKFlute analysis pipeline (Fig. 1B, Table S2)²⁶.

16

17 As expected, we identified editing of *UCK2*^{20,22}, which encodes the kinase that
18 converts AZA from nucleoside to nucleotide, as the top hit conferring resistance to AZA. We
19 also identified genes belonging to pathways involved in the DDR (*DYNLL1*, *ATMIN*, *BAX*),
20 tumor suppression (*FBXO11*, *GFI1B*), mRNA processing (*PSIP1*, *SMG9*, *DDX3X*), and
21 histone modification (*HDAC2*, *USP22*) as enriched hits. Fifty dropout gene targets
22 conferring hypersensitivity to AZA were identified. We focused on the sgRNAs depleted in
23 the AZA, but not vehicle, arm of our screen, as these their gene targets encode potential
24 combination drug ligands. Gene ontology terms, KEGG pathways, and WikiPathways
25 clustered dropout hits into key biological processes including excision DNA repair pathways,

1 protein SUMOylation, histone modification, and ubiquitin-like protein conjugating activities
2 (Fig. 1C). This was distinct from pathways significantly depleted in both AZA- and vehicle-
3 treated arms of the screen (Fig. S1C). AZA-dropout hits were ranked according to their
4 degree of depletion, revealing E2- and E3- ubiquitin ligases UBE2K and TOPORS, and the
5 ubiquitin-interacting protein UBXN7 as top dropout hits (Fig. S1D). To validate the impact
6 of individual gene perturbations on AZA sensitivity, two separate sgRNAs targeting each of
7 *UBXN7*, *UBE2K*, or *TOPORS* were individually transduced into MDS-L-Cas9. ICE
8 algorithm²⁷ analysis of Sanger sequencing across expected Cas9-cut sites revealed high
9 frequency polyclonal indels in the target genes with useful KO scores (Fig. S1E). Cellular
10 proliferation was assessed by tracking the frequency of tagRFP657-expressing cells over time
11 (Fig. 1D). In close concordance with our whole-genome screen, targeting *UBXN7*, *UBE2K*,
12 or *TOPORS* resulted significant depletion of tagRFP657+ cells under AZA selection,
13 validating these genes as *bona fide* drug target candidates that synergize with AZA therapy
14 (Fig. 1E).

15

16 ***Loss of TOPORS sensitizes leukemia cell lines to HMAs.***

17 Our top-ranked candidate was TOPORS. As an E3-ligase acting downstream of E1- and E2-
18 ligases in ubiquitylation and SUMOylation pathways²⁸⁻³¹, specific inhibitors of TOPORS
19 could be expected to have fewer undesirable side effects than inhibitors of E1- or E2-ligases,
20 making it the most attractive target from a theoretical therapeutic index standpoint. To test for
21 specific relevance to blood malignancies, gene expression was queried using the TCGA
22 database, which revealed that *TOPORS* is more highly expressed in human leukemia
23 compared to other cancer types (Fig. S2A).

24

1 We next determined the AZA dose-response relationship using *TOPORS*-edited
2 MDS-L cells across a range of AZA concentrations. Editing of *TOPORS* with two
3 independent sgRNAs (Fig. S1E) sensitized MDS-L-Cas9 cells to four consecutive days of
4 AZA treatment by up to 3.4-fold (Fig. 2A). For orthogonal validation, we generated MDS-L
5 lines lentivirally expressing shRNAs against *TOPORS* (Fig. S2B), which showed a similar
6 increase in sensitivity to AZA (Fig. 2B). Furthermore, enhanced sensitivity of *TOPORS*-
7 edited cells to AZA therapy was associated with a marked synergistic reduction in
8 clonogenicity (Fig. 2C).

9

10 As HMA therapy is used to treat a range of myeloid malignancies, we determined the
11 applicability of targeting *TOPORS* in AML. We generated three *TOPORS*-edited AML cell
12 lines (Fig. S2C) which reflect different stages of leukemic myeloid differentiation, including
13 MOLM-13 (*TP53*^{WT} AML line derived from a patient with antecedent HR-MDS), TF-1
14 (*TP53*^{WT} erythroleukemia line with del5q aberrations), and Kasumi-1 (*TP53*^{-/-} mutant
15 pediatric acute myeloblastic leukemia line). Polyclonal *TOPORS*-editing resulted in
16 significant increases in AZA sensitivity in all cell lines (Fig. 2D). Furthermore, enhanced
17 HMA-sensitivity conferred by *TOPORS*-editing extended to the 2'-deoxy derivative of AZA,
18 Decitabine (DAC) (Fig. S2D), implying that *TOPORS* acts downstream of drug incorporation
19 into DNA.

20

21 To evaluate the *in vivo* significance of our findings, we transduced *TOPORS*-edited
22 and control MOLM-13 cells with lentivirus encoding luciferase-GFP³², then transplanted
23 GFP⁺ sorted cells into cytokine-humanized adult “MISTRG” immune-compromised mice³³,
24 treated the mice for five consecutive days with AZA, and monitored disease progression
25 through bioluminescence imaging and event-free survival. In recipients transplanted with

1 *TOPORS*-edited MOLM-13 cells, a single five-day cycle of 1mg/kg i.p. AZA treatment
2 transiently reduced leukemia burden relative to controls by about 90% (Fig. 2E) and
3 significantly delayed disease progression (Fig. 2F).

4

5 ***Targeting TOPORS functionally spares healthy hematopoiesis.***

6 To assess the combination's relative toxicity to healthy cells, we used a hybrid
7 lentiviral/electroporation CRISPR gene-editing strategy³⁴ to edit *TOPORS* in human cord
8 blood CD34⁺ HSPCs (Fig. 3A), and confirmed effective polyclonal editing of the *TOPORS*
9 locus by indel frequency analysis (Fig S3A). We then treated sgTOPORS-1 edited CD34⁺
10 HSPCs with AZA or vehicle for five consecutive days in co-culture with murine MS5
11 stromal cells and carried out colony forming assays to assess HSPC function. *TOPORS*-
12 editing alone or in combination with AZA therapy did not impair colony forming capacities
13 compared to controls (Fig. 3B).

14

15 To assess the toxicity of targeting *TOPORS* *in vivo*, we transplanted *TOPORS*-edited
16 cord blood CD34⁺ HSPCs into neonatal MISTRG recipients³³ (Fig. 3C) and monitored
17 engraftment by tracking peripheral blood once the transplanted mice had reached adulthood,
18 and again after administering AZA at 1mg/kg for five consecutive days (a single treatment
19 cycle). Neither *TOPORS*-editing alone nor in combination with AZA treatment significantly
20 reduced the frequencies of circulating cells, relative to the non-targeting control (Fig. 3D),
21 although we did note long-term selection against engineered cells (i.e. tagRFP⁺ cells) in
22 favour of non-engineered (i.e. tagRFP⁻) human cells irrespective of the sgRNA (Fig. S3B).
23 After 8 weeks of recovery, we evaluated the combination of *TOPORS*-editing and DAC-
24 treatment (co-administered with the cytidine deaminase inhibitor tetrahydouridine [THU]),
25 on the same engrafted mice, by treating with 10mg/kg THU i.p. plus 0.1mg/kg DAC or

1 vehicle s.c. for two consecutive days per weekly cycle for a total of four cycles. This low
2 dose and frequency regimen, which minimizes metabolic adaptation and prolongs HMA-
3 sensitivity in the clinic^{3,5}, did not affect the production of *TOPORS*-edited blood cells relative
4 to control cells (Fig. 3D, Fig. S3B), nor did *TOPORS*-editing impact the survival of human
5 CD34⁺ progenitor cells in mouse bone marrow with or without sequential drug treatments
6 (Fig. 3E-F). Although variable between mice, the mean indel polyclonal KO scores for
7 *TOPORS*-edited human CD34⁺ cells exposed to HMA *in vivo* remained comparable to the
8 pre-treatment score, suggesting that *TOPORS* editing does not confer a selective
9 disadvantage on healthy human CD34⁺ cells (Fig. 3G). Unexpectedly, *TOPORS*-editing may
10 have biased towards accumulation of CD56⁺ NK cells in bone marrow of endpoint mice
11 regardless of HMA therapy, although this trend was not significant (Fig. S3C).

12

13 ***Targeting TOPORS primes HMA response in leukemic cells via deficient DDR.***

14 TOPORS, an Arg/Ser- (RS-) rich ring finger domain protein bearing SUMO interaction
15 motifs (SIM), was the first discovered dual ubiquitin and SUMO E3-ligase^{28,30}. TOPORS
16 activates DNA repair pathways by SUMOylating DNA repair factors and chromatin proteins,
17 including TP53, and down regulates the same pathways and overlapping factors *via*
18 ubiquitination; TOPORS is itself a SUMOylation substrate³⁵⁻³⁷.

19

20 We evaluated whether TOPORS participates in HMA-induced DDR by measuring
21 γ H2AX levels, a marker of DNA breaks, in AZA-treated MDS-L cells. Compared to control
22 cells, *TOPORS*-edited cells accumulated significantly more γ H2AX in response to AZA (Fig.
23 4A), indicating more DNA break persistence. This conclusion was supported by “comet”
24 assays, where DNA fragments from AZA-treated *TOPORS*-edited MDS-L cells migrated
25 during electrophoresis with larger tail moments compared to control cells (Fig. 4B). Flow

1 cytometry of fixed cells revealed that AZA-treated *TOPORS*-edited MDS-L cells
2 accumulated in late S- and/or G2/M phases (Fig. 4C–D), suggesting that AZA-induced DNA
3 damage delayed cell cycle progression of *TOPORS*-deficient cells subsequent to
4 incorporation of 5 aza-dC into DNA. Parallel annexin V co-staining revealed that AZA
5 treatment triggered higher levels of apoptosis in *TOPORS*-edited MDS-L cells compared to
6 control cells (Fig. 4E).

7

8 Because HMA incorporation into DNA is S-phase dependent, we used mass
9 spectrometry of digested DNA to test whether cell cycle changes induced by editing
10 *TOPORS* might alter either incorporation of 5 aza-dC into DNA, or subsequent DNA
11 demethylation³⁸. *TOPORS*-editing did not significantly change incorporation of 5 aza-dC into
12 DNA of cells treated with AZA but led to increased incorporation into DNA of cells treated
13 with DAC (Fig. 4F). Genome demethylation in response to 5 aza-dC incorporation was
14 similar in *TOPORS*-edited versus control cells (Fig. 4G).

15

16 ***Multi-omic approaches reveal widespread mis-splicing of DDR genes and cycle arrest in***
17 ***AZA-treated TOPORS-edited MDS-L cells.***

18 Besides its role in post-translational modification of proteins, *TOPORS* has also been
19 characterized as a transcriptional regulator through binding *cis*- regulatory elements and
20 influencing chromatin accessibility at enhancers^{39,40}. As these findings suggest that *TOPORS*
21 and AZA potentially converge through epigenetic remodelling and subsequent changes in
22 gene expression, we assessed the bulk transcriptomes and nuclear proteomes of *TOPORS*-
23 edited MDS-L cells treated with AZA. Gene set enrichment analyses revealed marked
24 enrichment of DNA replication and spliceosome transcriptional programs in AZA-treated
25 *TOPORS*-edited MDS-L cells compared to controls (Fig. 5A). Inference of transcriptional

1 regulatory networks underlying these alterations using the TRRUST database⁴¹ identified that
2 E2F1 targets significantly overlap upregulated genes in AZA-treated *TOPORS*-edited MDS-L
3 cells (Fig. 5B). Clustering of transcriptomes based on expression of E2F1 targets revealed
4 that AZA-treated *TOPORS*-edited MDS-L transcriptomes displayed the greatest enrichment
5 of E2F target genes (Fig. S4A). E2F1 is a transcription factor induced in response to DNA
6 damage, with major roles in cell cycle progression and DNA repair⁴². E2F1 localizes to sites
7 of DNA damage and origins of replication to collaborate with DNA repair proteins, enabling
8 DNA repair and completion of DNA replication⁴³. Thus, increased DNA replication
9 programs in AZA-treated *TOPORS*-edited MDS-L cells appear to be driven by increased
10 E2F1 activity.

11
12 Chemotherapeutics that induce DNA-adducts impair transcription through steric
13 hindrance⁴⁴. Bulky lesions in particular cause transcription-dependent splicing alterations⁴⁵
14 that result in use of weaker splice sites and facilitates the inclusion of suboptimal exons⁴⁶.
15 Therefore, AZA induced formation of bulky DNA-DNMT1 adducts could potentially impact
16 alternative splicing. Alternative splicing alterations can also be triggered by variations in
17 expression levels or post-translational modifications of splicing factors⁴⁷. According to the
18 BioPlex human interactome database⁴⁸, *TOPORS* interacts with splicing factors SRSF4 and
19 SRSF6 (Fig. S4B) and has been shown to SUMOylate other splicing factors³¹. For these
20 reasons, along with the enrichment of spliceosome signatures in AZA-treated *TOPORS*-
21 edited MDS-L cells, we investigated the alternative splicing landscape of these cells. We
22 used rMATs⁴⁹ to quantify five alternative splicing events from our bulk transcriptomic
23 datasets. Unsupervised hierarchical clustering and principal component analysis of all
24 samples revealed that AZA treatment and *TOPORS*-editing resulted in global splicing
25 alterations both individually and cooperatively (Fig. 5C).

1

2 We detected 764 mis-spliced events in AZA-treated *TOPORS*-edited MDS-L cells
3 compared to control cells, the majority being exon skipping events (n=473, FDR <0.05,
4 PSI>0.1) (Fig. 5D). Over-representation analysis associated these mis-spliced genes with
5 pathways relating to the DDR (Fig. 5E). To test whether specific RNA binding proteins were
6 responsible for these exon skipping events, we used rMAPs⁵⁰ to assess the density of RNA
7 binding protein motifs within the associated sequences. We identified significant enrichment
8 for a motif (AGCGGA) bound by SRSF6, a spliceosome factor known to interact with
9 *TOPORS* in HEK293 cells⁴⁸. Exons 3' to this motif were differentially retained in AZA-
10 treated *TOPORS*-edited MDS-L cells (Fig. 5F). We also identified significant enrichment for
11 two SRSF1 binding motifs but did not identify any specific enrichment for SRSF4 motifs
12 (Fig. S4C). Defective SRSF6-dependent DDR transcript splicing might therefore be a
13 contributing factor to the AZA sensitivity of *TOPORS*-edited MDS-L cells.

14

15 Since *TOPORS* is primarily nuclear-localized, we profiled the nuclear proteome of
16 AZA-treated and *TOPORS*-edited MDS-L cells using label-free mass spectrometry. On
17 average, 1500 proteins were detected per sample with a minimum coverage of 1000 proteins
18 between samples (Fig. S5A). Similar to our transcriptomics data, AZA-treated *TOPORS*-
19 edited cells had a distinct nuclear proteome compared to controls (Fig. S5B). Differential
20 abundance analysis identified 73 of 2257 proteins as significantly differentially abundant
21 across all samples (Fig. 6A). After hierarchical clustering, cluster 1 represented proteins that
22 were down-regulated specifically in steady state cells by *TOPORS* activity – presumably via
23 *TOPORS*-mediated ubiquitination. Clusters 4 and 6 represented proteins that were enriched
24 or depleted, respectively, in AZA-treated *TOPORS*-edited MDS-L cells (Fig. 6A). Over-
25 representation analyses indicated that cluster 4 proteins were associated with late-stage cell

1 cycle proteins, while cluster 6 proteins were associated with global nucleotide excision repair
2 pathways (Fig. 6B). DNMT1 (bottom of cluster 5) was significantly depleted in AZA-treated
3 MDS-L cells, regardless of *TOPORS* editing (Fig. 6B). This was also so in DAC-treated
4 MOLM-13 cells (Fig. 6C), indicating that *TOPORS*-deficiency did not prevent HMA-
5 induced depletion of DNMT1. The notably higher levels of protein SUMOylation we
6 observed in DAC-treated *TOPORS*-edited MOLM13 cells (Fig. 6C), indicated that *TOPORS*
7 was not needed for DNA damage-induced SUMOylation generally. Nonetheless, our finding
8 that DNMT1 levels in AZA-treated *TOPORS* edited cells were two-fold higher compared to
9 the AZA control (t-test p=0.03; Fig. 6B), indicated that AZA-induced DNMT1 degradation
10 might be specifically influenced by *TOPORS* activity. Overall, our transcriptomic and
11 proteomic findings were consistent with the impaired DNA damage and cell cycle arrest
12 signatures identified in functional assays and indicated that *TOPORS*-deficiency might
13 synergize with AZA both by impeding the removal of AZA-induced DNMT1-DNA adducts
14 and by altering RNA splicing during AZA-induced DDR.

15

16 ***TOPORS*-editing sensitizes cells to HMA in a DNMT1-dependent manner.**

17 To formally test whether genome demethylation *per se* or DNMT1 were involved in HMA-
18 hypersensitivity in *TOPORS*-edited cells, we measured sensitivity to a novel DNMT1 small
19 molecule inhibitor (GSK3685032) which inhibits DNMT1 without incorporating into nucleic
20 acids⁵¹. *TOPORS*-edited cells were not more sensitive to GSK3685032 than control cells,
21 even at GSK3685032 concentrations inducing very high levels of cytidine demethylation
22 (Fig. 7A). We formally tested whether DNMT1 was involved in MDS-L HMA-sensitivity by
23 exposing cells to DAC in the presence or absence of 1μM GSK3685032, a concentration
24 which induced near-maximal DNMT1 inhibition with minimal cytotoxicity (Fig. 7A, Fig.
25 7B). DAC-mediated killing of both *TOPORS*-edited and control MDS-L cells was reduced

1 equally (by 7.4-fold; Table S3) in the presence of 1 μ M GSK3685032, implicating DNMT1
2 adduction as the dominant cytotoxic event in DAC-treated MDS-L cells, regardless of
3 TOPORS activity. To test whether other replication-blocking DNA-protein adducts require
4 TOPORS for efficient resolution, we assessed sensitivity to the topoisomerase inhibitors
5 topotecan or etoposide, which prevent type 1 or type 2 topoisomerases from resolving the
6 transient tyrosine-DNA ester bonds they form with DNA. *TOPORS*-editing did not sensitize
7 MDS-L cells to either topoisomerase I or II inhibition by a single dose of topotecan or
8 etoposide (Fig. 7C-D), and furthermore did not sensitize to hydroxyurea – a ribonucleotide
9 reductase poison that disrupts nucleotide synthesis (Fig. 7E). Thus, TOPORS-deficiency
10 sensitizes to DNA-DNMT1 adducts specifically, and not to disrupted nucleotide metabolism
11 nor to DNA-protein adducts in general.

12

13 ***TOPORS*-editing does not reduce SUMOylation of DNMT1 in HMA-treated AML cells.**

14 DNMT1 SUMOylation followed by RNF4-mediated SUMO-targeted ubiquitylation
15 are critical for clearance of HMA-induced DNMT1 adducts^{52,53}. This lead us to suspect that
16 TOPORS may mediate DNMT1 SUMOylation, but the potential importance of interactions
17 between TOPORS and other targets, such as RNA-splicing factors, prompted us to explore
18 TOPORS' E3 SUMO-ligase activity in an unbiased manner in AML cells. *TOPORS*-edited or
19 control MOLM-13/Cas-9 cells were engineered to co-express Dasher-GFP plus SUMO1 N-
20 terminally tagged with 10xHis (10His-SUMO1, Fig. S6A). Sorted Dasher-GFP+ cells were
21 treated for 3 consecutive days with 4.2 nM DAC or vehicle then whole cell guanidine-
22 extracted proteins bearing 10xHis tags were enriched by pull-down with Ni-NTA beads⁵⁴,
23 and subjected to label-free LC-MS/MS analyses. Mass spectral yields for 10xHis-enriched
24 proteins were substantially lower and more variable between replicates than for our prior
25 nuclear proteomics (Fig. S5; Fig. S6B–C). Nonetheless, a small set of Ni-captured proteins,

1 including DNMT1, were significantly differentially abundant across the four experiment
2 conditions, (Fig. S6D). One of the highest ranked Ni-captured proteins depleted from
3 *TOPORS*-edited cells, regardless of DAC treatment, was *TOPORS* itself (Fig. S6D, Fig. 8A–
4 C). This unequivocally confirmed that *TOPORS*-editing had substantially depleted *TOPORS*
5 protein and/or its E3 SUMO-ligase activity from AML cells. Other proteins differentially
6 captured by Ni-NTA from vehicle-treated (steady state) cells were likely E3-ligase targets of
7 *TOPORS*; these were predominantly involved in ribonucleoprotein complex biogenesis and
8 in RNA splicing (Fig. 8D), which was strikingly consistent with our prior transcriptome and
9 nuclear proteome datasets. Focusing on DNMT1, SUMOylated DNMT1 was almost equally
10 Ni-NTA captured from DAC-treated control and *TOPORS*-edited cells, but not from vehicle-
11 treated cells (Fig. 8C). Since total DNMT1 levels drop substantially in MDS/AML cells
12 chronically treated with low dose HMA, regardless of *TOPORS* activity (Fig. 6B–C), we
13 deduce that the SUMOylation level of the remaining DNMT1 was very high, and that
14 *TOPORS* is not required for HMA-mediated DNMT1 SUMOylation. Indeed, our prior
15 orthogonal experiments indicated that the levels of SUMOylated DNMT1 were higher in
16 HMA-treated *TOPORS*-edited compared to controls. Furthermore, our combined data
17 indicate that reduced *TOPORS*-mediated SUMOylation or ubiquitylation of proteins involved
18 in RNA metabolism and splicing (Fig. 8D) likely plays an important role in the sensitivity of
19 *TOPORS*-edited cells to HMA.

20

21 ***SUMOylation blockade synergizes with HMAs in MDS and AML in vivo.***

22 Concurrent with pursuing the mechanistic basis of synergy between *TOPORS*-editing
23 and HMAs, we evaluated whether our findings are translatable to clinical application. There
24 are currently no pharmacological molecules specifically inhibiting *TOPORS*. However, the
25 prior known importance of SUMOylation in clearing HMA-induced DNMT1 adducts

1 suggested that inhibiting SUMOylation might enhance the potency of HMA therapy. The
2 first-in-class drug TAK-981 acts upstream of SUMO E3-ligases such as TOPORS by
3 preventing attachment of SUMO to the universal SUMO E2-conjugase UBC9, which leads to
4 global inhibition of protein SUMOylation⁵⁵. Combinatorial treatment with TAK-981 and
5 AZA was cytotoxically additive in MDS-L and Kasumi-1 (both *TP53* mutant), but synergistic
6 in MOLM-13 and TF-1 cell lines (both *TP53* wild-type, Fig. 9A and Fig. S7A). Critically,
7 TAK-981 and DAC combination was synergistic in all four cell lines (Fig. 9B and Fig. S7B).
8 Lower synergism with AZA may reflect SUMO-independent activities mediated by drug
9 incorporation into RNA, which are not replicated by DAC. We also measured the impact of
10 low concentration TAK-981 (0.1μM) on HMA cytotoxicity in *TOPORS*-edited versus control
11 MDS-L cells. The difference in HMA-sensitivity between control and *TOPORS*-edited cells
12 was much smaller in the presence of TAK-981 (AZA:1.2-fold, DAC: 1.4-fold) compared to
13 its absence (AZA: 1.99-fold, DAC: 1.94-fold Fig. 9B, Fig. 9C, Table S4), demonstrating that
14 TOPORS mediates a substantial proportion of SUMO-dependent survival in HMA-exposed
15 MDS-L cells. To determine whether TAK-981 could phenocopy the DDR-deficient signature
16 induced by *TOPORS*-editing, we treated MDS-L with the lowest synergistic dosage of TAK-
17 981 and HMAs (from synergy maps in Fig. S7) and assessed γH2AX levels and cell cycle
18 status. Low-dose TAK-981 combined with low-dose HMA resulted in extensive
19 accumulation of γH2AX with concomitant accumulation of cells in the late S and G2/M
20 phases (Fig. 9D-E).

21

22 We next asked whether *in vitro* synergy between TAK-981 and HMAs extended to a
23 more clinically relevant *in vivo* context. TAK-981 combined with low dose AZA
24 synergistically and significantly prolonged survival in MISTRG mice engrafted with MOLM-
25 13 cells (Fig. 9F). To determine whether TAK-981 also sensitizes primary patient AML cells

1 to AZA *in vivo*, we transplanted patient-derived continuous xenograft (PDX) lines AML-5
2 and AML-16⁵⁶ into MISTRG mice, followed by drug treatment (Fig. 9G–J). Expansion of
3 these PDX was significantly delayed by AZA therapy alone, but not by TAK-981 alone, and
4 expansion was synergistically delayed by combined AZA plus TAK-981 therapy (Fig. 9G–J).

5

6 Finally, to test the impact of combined TAK-981 and AZA treatment on healthy cells
7 we injected escalating doses of TAK-981 i.p., combined with AZA s.c., into adult MISTRG
8 mice engrafted with cord blood CD34⁺ cells (Fig. S8A). The frequencies of
9 huCD45⁺moCD45⁻ cells amongst all CD45⁺ cells in MISTRG bone marrow were determined
10 by cytometry at endpoint and revealed no significant differences between treatment groups in
11 endpoint levels of human CD45⁺ cell persistence (Fig. S8B). Thus, combined TAK-981 and
12 HMA treatment is preferentially effective against leukemic cells whilst sparing healthy blood
13 stem and progenitor cells *in vivo*.

14

15

1 **DISCUSSION**

2 In this study, we established a role for the dual E3 ubiquitin and SUMO ligase TOPORS as a
3 central regulator of the DDR induced by incorporation of 5 aza-dC into DNA. We provide
4 genetic proof of concept that targeting TOPORS confers hypersensitivity to HMAs through
5 predisposing leukemia cells to a defective response to DNA-DNMT1 adducts. This
6 hypersensitive phenotype was not dependent on the *del5q* or *TP53* mutational status.
7 Furthermore, we demonstrate that these therapeutic benefits extended to an *in vivo* AML
8 model and that TAK-981 is a viable pharmacological surrogate to targeting *TOPORS*. Our
9 work taken together with reports published during the course of this research suggests that
10 TAK-981 combined with HMAs could offer therapeutic benefits to HR-MDS and AML
11 patients⁵⁸.

12

13 By integrating functional and multi-omic approaches, we show that both *TOPORS*-
14 editing and TAK-981 treatment prime an HMA sensitivity phenotype through impairing the
15 DDR to HMA-induced DNA-DNMT1 adducts. Synergy of TAK-981 was higher with DAC
16 compared to AZA, especially in *TP53*-mutant cells. Although TAK-981 is an effective
17 surrogate for TOPORS-editing and demonstrates cytotoxic synergism in combination with
18 low dose HMAs, it should be noted that reduction in TOPORS activity synergizes with
19 HMAs much more specifically than reduction in upstream SUMOylation activity mediated
20 by TAK-981. Complete inactivation of SUMOylation is lethal, while inactivation of E3
21 ligase TOPORS alone is not⁵⁹. Indeed, in the absence of AZA, MDS-L proliferation in our
22 initial CRISPR-Cas9 screen was reduced in *UBC9*-edited, but not in *TOPORS*-edited cells,
23 while proliferation in the presence of AZA was highly dependent on both *UBC9* and
24 TOPORS activities (Table S2). Thus, TOPORS is an attractive target for development of
25 specific inhibitors with potentially improved therapeutic index compared to TAK-981.

1

2 Beyond its extensive role in modulating the DDR, SUMOylation plays a crucial role
3 in transcriptional repression of inflammatory cytokines via its influence on chromatin
4 architecture⁶⁰. TAK-981 monotherapy was shown to promote inflammatory anti-tumor
5 immune responses through re-activation of a type I interferon response, and potentiating
6 response to immune checkpoint blockade⁵⁵. These findings align with previous reports where
7 HMA treatment of solid tumors triggered de-repression of silenced endogenous retroviral
8 elements resulting in a potent anti-tumor inflammatory response^{17,18}. However, it is unlikely
9 that TAK-981 and HMAs are converging through inflammatory pathways in MDS/AML
10 cells, because these pathways were not enriched in our or other^{20,21} screening datasets, and
11 expression levels of inflammatory pathways do not reliably predict patient response⁶¹. These
12 findings suggest that either; (1) the level of redundancy in these inflammatory pathways are
13 not conserved between solid tumors and hematopoietic malignancies; (2) the relative
14 expression of these independent inflammatory factors in each model plays a role in HMA
15 dependencies; or (3) these inflammatory pathways primarily modulate HMA response in
16 either a non-proliferative or HSPC-extrinsic manner, readouts that were not captured from
17 our screening efforts.

18

19 We confirmed DNMT1 as the dominant mediator of HMA cytotoxicity in AML cells,
20 consistent with previous findings in other tumor models. Against our initial expectations, we
21 found that TOPORS was not required for SUMOylation of adducted DNMT1. However,
22 HMA-induced DNMT1 degradation was nonetheless reduced in *TOPORS*-edited cells.
23 Parallel investigations by others performing similar CRISPR screens identified TOPORS as a
24 SUMO-targeted ubiquitin E3 ligase that acts in semi-redundant concert with RNF4 to
25 mediate efficient proteasomal degradation of DNA-adducted DNMT1^{62,63}. Nonetheless, our

1 data strongly indicate that ubiquitylation of SUMOylated DNMT1 adducts is not the only
2 mechanism by which TOPORS protects HMA-exposed cells from DDR-induced apoptosis.
3 Our proteomics identified RNA splicing factors as key candidates for TOPORS-mediated
4 SUMOylation or ubiquitylation in AML cells, even in the absence of HMA, and
5 characterized widespread mis-splicing of DNA repair genes in TOPORS-edited cells, likely
6 due in part to aberrant SUMO- or ubiquitin-modulation of interacting splicing factors. These
7 results draw similarities to a recent study which showed that splicing modulators targeting
8 SF3B1 triggered enhanced exon-skipping in DNA damage repair genes⁶⁴. Widespread mis-
9 splicing of DNA repair genes impaired the DDR in cohesin-mutant AML cells by altering
10 repair protein function, providing a novel approach to sensitize cancer cells to
11 chemotherapeutics and PARP inhibitors. We speculate that targeting TOPORS produces
12 similar deficits in DDR proteins via mis-splicing, and it would be worthwhile to determine
13 whether HMAs could also be combined with splicing modulators for therapeutic benefit.

14

15 TOPORS is a promising drug development candidate for HMA combinatorial therapy
16 because TOPORS-editing did not impair S-phase-dependent HMA incorporation into DNA
17 and did not significantly impair blood-forming capacities *in vitro* or *in vivo*. We speculate
18 this was due to greater redundancy between RNF4- and TOPORS-dependent DNA-DNMT1
19 adduct clearance⁵³ in healthy compared to leukemic cells. Our findings that DNMT1
20 inhibition caused a larger fold-change in DAC-sensitivity in MDS-L cells than inactivation of
21 TOPORS, and that *TOPORS*-editing did not prevent DNMT1-depletion in chronically HMA-
22 treated MDSL/AML cells, demonstrate that such redundancy for DNA-DNMT1 adduct
23 resolution is evident even in leukemic cells.

24

1 Our data contrast previous clinical studies where other inhibitors of post-translational
2 mechanisms, including the proteasomal inhibitor Bortezomib (NCT00624936,
3 NCT01420926)⁶⁵ or Pevonedistat (inhibitor of NEDD8 Activating Enzyme) in combination
4 with AZA⁶⁶ did not provide a survival advantage over AZA monotherapy. A possible
5 explanation for these results could be that these agents exhibit strong anti-mitotic properties,
6 which might antagonize incorporation of HMAs into tumor DNA^{67,68}. In immune sufficient
7 AML patients, an added benefit of TAK-981 combination therapy may be its potential to
8 activate anti-tumor T and NK cells^{55,69}. While TOPORS is currently not druggable directly,
9 in the interim we propose low dose HMA in combination with TAK-981 as a viable
10 therapeutic strategy to be considered for HR-MDS and AML.

11

12

1 **METHODS**

2

3 **Human specimens**

4 Cord blood units were supplied by Sydney Cord Blood Bank under the approval of the South
5 Eastern Sydney Local Health District (reference 08/190). Mononuclear cells isolated using
6 lymphoprep (ELITech Group, #1114547), and CD34+ cells were enriched using magnetic
7 beads (Miltenyi Biotec, #130-046-702) on an autoMACS Pro Separator (Miltenyi Biotec)
8 according to manufacturer's instructions.

9

10 **Cell culture and drug treatments**

11 Cell cultures were grown in a humidified incubator at 37°C supplemented with 5%
12 CO₂. All leukemia cell lines were maintained in RPMI 1640 medium (Life Technologies,
13 11875-093) containing 10%-20% fetal bovine serum (FBS) (Sigma-Aldrich, F9423-500mL)
14 supplemented with 1X GlutaMAX (Gibco, 35050-061) and 100units/mL of penicillin-
15 streptomycin (Gibco, #15140-122). MDSL and TF-1 were additionally supplemented with
16 25ng/mL of recombinant human IL-3 (Miltenyi Biotec, 130-095-069), and MDS-L with
17 50nM β-mercaptoethanol (Sigma-Aldrich, #M6250-100mL). MS5 cells were maintained in
18 Gibco's α modified eagle's medium (Gibco, #12571063) supplemented with 10% FBS. The
19 identity of all leukemia cell lines was confirmed by STR profiling at the Garvan Institute of
20 Medical Research and routine mycoplasma testing was performed at the Mycoplasma Testing
21 Facility, UNSW Sydney. The MDS-L cell line was a generous gift from Dr. Kaoru Tohyama
22 (Department of Laboratory medicine, Kawasaki Medical School).

23 Unless otherwise specified, cells were treated *in vitro* with AZA (Selleck, # S1782),
24 DAC (Selleck, #S1200), TAK-981(Selleck, #S8829 [*in vitro* use] or Takeda [*in vivo* use]),
25 Topotecan (Sapphire BioScience cat. A10939-50 , Etoposide (Clifford Hallam Healthcare,

1 cat. 1280860), Hydroxyurea (Selleck, #74-S1896) or GSK3685032 (Selleck cat. E1046) at
2 the indicated concentrations daily for 4 days.

3

4 **Capture panel Genotyping**

5 Genotyping of MDS-L and PDX AML-5 was performed as previously described using a
6 capture panel of 111 genes relevant to myeloid malignancies⁷⁰.

7

8 **Viral transduction and generation of stable cell lines**

9 pLeGO-iG2-Luc was a gift from Dr Kristoffer Weber³². pLKO5d.SFFV.SpCas9.p2a.BSD
10 (Cas9-BsD) was used to generate Cas9-expressing cell lines. The following sgRNA
11 sequences were cloned into SGL40C.EF879S.tagRFP657: AACGGCTCCACCACGCTCGG
12 (sgROSA/CONTROL), CCATGGTGCCTGACTAACAG (sgTOPORS-1),
13 GGACAGTTCAACAAGTTCTG (sgTOPORS-2), TAATATTAGTTCCGTACAG
14 (sgUBE2K-1), GCAATGACAATAATACCGTG (sgUBE2K-2),
15 ACAGGTTTATCATGACAGTG (sgUBXN7-1), TCAGGTGCAAGTGAAAGTGT
16 (sgUBXN7-2). shRNA lentiviral vectors were purchased from GeneCoiepoeia:
17 GCTTCGCGCCGTAGTCTTA (shCONTROL), GGGCAGAAGATGACTTCAAGG
18 (shTOPORS-1), GCATGATCAGAAGAATCATAG (shTOPORS-2).

19

20 Non-replicating lentiviruses were produced in HEK293T cells using the 2nd
21 generation packaging plasmids psPAX2 construct (Addgene #12260), pMD2.G construct
22 (Addgene #12259), and the respective lentiviral transfer plasmid. Lentiviral supernatant
23 supplemented with 8ug/mL polybrene was used for transduction into the respective cell lines.

24

25 **ICE Analysis**

1 Genomic DNA was harvested from sgRNA-transduced cells using either the Monarch
2 genomic DNA purification kit (NEB, #T3010S) or QuickExtract DNA extraction solution
3 (Lucigen, #QE0905T) according to manufacturer's instructions. Genomic regions flanking
4 the expected cut sites for the indicated sgRNAs were PCR amplified using Q5 PCR Master
5 Mix (NEB, #M0541L). PCR products were purified using the Monarch PCR and DNA
6 Cleanup Kit (NEB, #T1030L) prior to Sanger sequencing. Primers for amplification and
7 sequencing were as follows; TOPORS-1: F-TGCCTTCACAGATTAGTCCCCTGG, R-
8 GCCCACTTCTACTCTGAGAACGTG, Seq-TGGAGAGTCAGGCATTGTGTCTG,
9 TOPORS-2: F-TGCCTTCACAGATTAGTCCCCTGG, R-
10 GCCCACTTCTACTCTGAGAACGTG, Seq-TGCCCTGCTCCTTCATACGAAG, UBXN7-
11 1: F-TGGGAAAGGAGGAGGAATGGGTC, R-CGGGTTCAGGCCATTCTCCTGC, Seq-
12 TGCAATTCTGAAAACAGATCCAGTC, UBXN7-2: F-
13 GCCTCAGCCTCCCAAGGTGTTG, R-GCAGAGCACCACCACACTCC, Seq-
14 GGCAATGGATAGCTCCTGACAACAC, UBE2K-1: F-
15 CTGCACCCCTGCCTCACATGAAG, R-TGTGCTCAATTAAACACAACCTGC, Seq-
16 ACACCCCTTCTTCACCTAGGC, UBE2K-2: F-CCAGCACATTGGGAGGCCAAGG, R
17 GCAGGGAGGGATCATCACTGAAAGG, Seq-AGAGCCAGACTCCGTCTCAGGG.
18 Sequencing traces (.ab1 format) for gene-edited and corresponding wild-type were uploaded
19 to Synthego's inference of CRISPR edits server for indel analysis
20 (<https://ice.synthego.com/#/>).

21

22 Dropout Screen

23 Cas9-expressing MDS-L cells were infected with lentivirus encoding the human Brunello
24 CRISPR knockout pooled library (concentrated lentiviral aliquots were purchased from the
25 Victorian Centre for Functional Genomics, generated from Addgene# 73178) in the presence

1 of 8 μ g/mL polybrene at a multiplicity of infection of ~0.3. After 72h, library transduced
2 MDS-L-Cas9 cells were selected with 1 μ g/mL puromycin for 5 days then left to recover for
3 72 hours to allow for maximum gene editing. At time-0, ~5 \times 10⁷ live cells were harvested per
4 replicate and cell pellets underwent same-day nuclei preparation using Qiagen Blood & Cell
5 Culture DNA Maxi Kit (Qiagen, #13362) according to the manufacturer's instructions.
6 4.5 \times 10⁶ cells were also harvested and stained for CellTrace staining according to the
7 manufacturer's instructions to track cellular proliferation in parallel throughout the screen.
8 For dropout screening, Brunello-transduced MDS-L-Cas9 cells were split into 2 treatment
9 arms: AZA (0.3 μ M) or vehicle (DMSO, 0.000003%). AZA or vehicle was refreshed daily,
10 and cells were passaged every 3-4 days. A minimum of 3.9 \times 10⁷ cells for each replicate and
11 condition were maintained at every passage to preserve library representation. Endpoint cell
12 samples were harvested when the AZA-treated arm underwent 12 cellular divisions as
13 determined by CellTrace staining (alternate colored at each passage). Approximately 6-
14 15 \times 10⁷ cells were harvested for each endpoint samples. sgRNA cassettes were PCR amplified
15 across multiple 50 μ L reactions, each containing 5 μ g gDNA, using staggered P7 primers and
16 indexed P5 primers, and 2X NEBNext Q5 high fidelity master mix (NEB, #M0541L) as
17 previously described^{25,71}. PCR products were pooled, purified using AMPure XP beads, and
18 1.0pM of the pooled CRISPR libraries were sequenced on the NextSeq 500 platform using
19 the NextSeq 550 high-output kit with a read length of 1 x 75bp and a 20% PhiX spike-in.
20

21 The MAGeCKFlute pipeline was used for processing CRISPR screen data, quality
22 control, and hit identification²⁶. Briefly, CRISPR screen data was pre-processed using
23 MAGeCK's (Version 0.5.9.2) count function with standard parameters to generate sgRNA
24 count tables. Hit identification was performed using MAGeCK MLE (Version 0.5.3) using
25 standard parameters using a 3-condition design (day 0, drug treatment, and DMSO

1 treatment). Functional analysis and visualization of the MAGeCK MLE results were
2 performed using MAGeCkFlute (Version 1.14.0) with standard parameters and normalized
3 with the cell cycle parameter. ClueGO (Version 2.5.9) was used to generate dropout hit
4 cytoscape plots using integrated gene ontology, KEGG, and WikiPathway terms.

5

6 **CD34 editing and coculture**

7 Cord blood-derived HSPCs were gene-edited for *TOPORS* or control (sgROSA) using the
8 combined sgRNA-lentiviral and Cas9-mRNA electroporation approach as previously
9 described³⁴.

10 For transduction, lentiviral supernatants were loaded in RetroNectin-coated plates
11 then centrifuged at 1000 x g for 90mins at room temperature. After washing plates, 2mL of
12 CD34⁺ cells were added at a density of 1-2x10⁵ cells/mL and incubated for 72 hours in a
13 37°C incubator. Transduced cells (tagRFP657⁺) were sorted for CD34⁺ using anti-human
14 CD34-PE antibody (BD Biosciences, # 555822) on the FACS AriaIII (Becton Dickinson),
15 then electroporated with GFP-Cas9 mRNA (Dharmacon, #CAS11860) using a Neon
16 electroporator (Invitrogen). Electroporated cells were immediately transferred to 0.5ml pre-
17 warmed media in a 24-well plate and returned to the 37°C incubator. Transfection efficiency
18 was checked by GFP expression 16-24 hours after electroporation and gene editing
19 efficiencies were checked 4-5 days after transfection. Efficient editing of the *TOPORS* locus
20 was confirmed through ICE analysis from approximately 10000 cells per sample.

21

22 24 hours after combinatorial transduction and electroporation was performed, 10000
23 *TOPORS*-edited or control CD34⁺ cord blood-derived HSPCs were seeded into 24-well
24 plates in an MS5 co-culture system. Briefly, MS5 cells were plated into 24-well plates with
25 1.5x10⁵ cells/well and left to form a confluent monolayer overnight. CD34⁺ cells were then

1 plated onto MS5 monolayer in MyeloCult H5100 media (Stemcell Technologies, #05150)
2 and cells treated with 0.5 μ M AZA for 4 consecutive days. On Day 5, cells were collected
3 from culture plates and sorted for human CD34 $^{+}$ cells. MS5 cells were excluded using anti-
4 mouse CD105-eFluor450 antibody (Invitrogen, #48-1051-82).

5

6 **Colony forming assay**

7 1000 sorted CD34 $^{+}$ cells, or 1000 MDS-L cells were seeded per 1mL of MethoCult H4434
8 (StemCell Technologies, #04434) in 35mm dishes. Healthy colonies were scored after 10-14
9 days according to manufacturer's instructions. MDS-L primarily produce CFU-GM. Only
10 colonies greater than 40 cells were scored.

11

12 **Competitive proliferation assay**

13 Cas9-expressing MDS-L cells were transduced with sgRNA/tagRFP657 $^{+}$ lentiviral constructs
14 and were left unsorted for tagRFP. Cells were treated daily with 0.3 μ M AZA or DMSO for
15 16 days. The proportion of tagRFP657 $^{+}$ cells were measured using the BD LSRFortessa
16 SORP at pre-treatment levels and every 4 days up until day 16.

17

18 **EC50 measurements**

19 Cells seeded in 96-well plates were exposed to inhibitors at indicated concentrations.
20 Following drug treatment, DAPI was added to each well to a final concentration of
21 0.25 μ g/mL. Plates were analyzed on the Attune NxT (Invitrogen) using the 96-well sampler
22 with fixed volume analysis to record the absolute number of DAPI $^{-}$ and fluorescent protein
23 positive cells (tagRFP657 $^{+}$ for sgRNA-transduced samples; GFP $^{+}$ for shRNA-transduced
24 samples). Dose-response curves were fitted using the log(inhibitor) vs normalized response
25 4-parameter variable slope in GraphPad Prism (v10.1.1).

1

2 To test drug synergy, cells were treated with inhibitor in a 2D dose matrix, and
3 viability determined by MTS assays (Promega, #G5430). Synergy scores were calculated
4 using <https://synergyfinder.fimm.fi/>. ZIP scores less than -10 indicated an antagonistic
5 interaction between both drugs, from -10 to 10 indicated an additive interaction, and greater
6 than 10 indicated a synergistic interaction between both drugs.

7 **Apoptosis analysis using annexin V/Propidium Iodide (PI)**

8 Apoptosis analysis by Annexin V/PI staining was performed using Abcam's Annexin V-
9 FITC kit (Abcam, #ab14085) according to the manufacturer's instructions.

10

11 **γ H2AX and cell cycle flow cytometry**

12 Cells were washed, fixed with 4% formaldehyde in PBS for 10 minutes at room temperature,
13 permeabilized with ice-cold 90% v/v methanol and incubated for 5 minutes at room
14 temperature, then resuspended in FACS buffer (2% FBS, 1mM EDTA in PBS); all in the dark
15 or low lighting.

16

17 For γ H2AX staining, cells were blocked using human Fc Block (BD, #564220) then
18 stained with γ H2AX antibody (2 μ g/mL, Abcam, #ab26350) for 1 hour at room temperature,
19 followed by anti-mouse DyLight 488 antibody (1:500 in 0.1% NP40/PBS, Abcam,
20 #ab96879) for 30 minutes at room temperature; all in the dark or low lighting. Cells were
21 analysed on the LSRFortessa SORP.

22

23 For cell cycle analysis, fixed cells stained with DAPI (1 μ g/mL, BD Biosciences,
24 #564907) were analyzed on the LSRfortessa SORP with V450 and UV450 channels set to

1 linear. Samples were run at low speed and voltages adjusted until the G1 peak sat as close to
2 100 as possible. Data was analyzed on FlowJo (Version 10.7.1) applying the Dean Jett Fox
3 pragmatic model.

4

5 **Comet Assay**

6 Cell pellets were washed once with ice-cold PBS (without Mg²⁺ and Ca²⁺), then
7 resuspended at 1x10⁵ cells/mL in ice-cold PBS and analysed using the comet assay kit
8 (Abcam, #ab238544) according to manufacturer's instructions with gel electrophoresis run
9 for 20 minutes at 3 volts/cm.

10

11 **RNA Seq and data analysis**

12 Total RNA was extracted using the Bioline Isolate II RNA extraction Kit (Bioline, BIO-
13 52072) according to the manufacturer's instructions. Residual DNA was eliminated by using
14 the RNase-free DNase Qiagen Kit (Qiagen, #79254). RNA-seq libraries were prepared using
15 the Illumina Stranded mRNA prep Ligation kit performed as per manufacturer's instructions
16 and libraries sequenced on the NovaSeq 6000 platform using 1 lane of a 2 x 100bp SP flow
17 cell.

18

19 Raw FASTQ files assessed for quality control through FastQC and sequencing
20 adaptors and low quality reads removed using BBmap. Paired-end reads were mapped to the
21 hg38 reference genome using STAR (Version 2.7.0) and quantified using featureCounts
22 (Version 2.0.0). The parameters “--outFilterMismatchNoverLmax” and “--alignEndsType” of
23 STAR (Version 2.7.0) aligner was set to “0.05” and “EndToEnd” to filter out reads
24 harbouring artifact mismatches from the mapping process. Read count matrices were

1 generated with FeatureCounts using default arguments with “requireBothEndsMapped” and
2 “countChimericFragments” options.

3

4 rMATS (Version 4.1.2) was used to detecting splicing events and differentially
5 splicing⁴⁹. Spliced events were filtered using an FDR cut-off of less than 0.05 and inclusion
6 level difference greater than |0.1|. Five types of splicing events were captured: exon skipping,
7 Intron retention, alternative 3' splice site, alternative 5' splice site, and mutually exclusive
8 exons.

9

10 Unsupervised hierarchical clustering analysis was used to assess the power of
11 differentially spliced events in separating samples of different comparisons aligned with their
12 labels (MRAZA, MRDMSO, MT1AZA and MT1DMSO). First z-score normalization was
13 performed on processed Inclusion Level table to adjust for the signal to noise ratio. The K-
14 means algorithm was used to perform unsupervised hierarchical clustering on both genes and
15 labels. The number of K for labels was set to four. To obtain a consensus k-means clustering,
16 100 k-means runs were executed for both labels and genes simultaneously.

17

18 To identify differentially expressed genes, DESeq2 R package (Version 1.34.0) was
19 used. First gene count tables were normalized and genes with normalized read counts less
20 than 10 were filtered out. RNA binding factor motif density scanning was performed using
21 the RMAPs2 server (<http://rmaps.cecsresearch.org/#about-section>)⁵⁰. Raw outputs from
22 rMAPS were uploaded onto the server and analyzed for RNA binding factor motif densities
23 using default settings. Overrepresentation and transcription factor regulatory target analyses
24 were performed using the MetaScape server (<https://metascape.org/gp/index.html>). Filtered

1 lists (FDR< 0.05, |Log₂Fold-Change|>1) were uploaded for express analysis.

2

3 **Quantitative RT-PCR**

4 RNA was reverse transcribed into cDNA using the QuantiTect reverse transcription kit
5 (Qiagen, #205311) as per manufacturer's instructions. cDNA was amplified PowerUP SYBR
6 green master mix (Applied Biosystems, #A25776) on a BioRad CFX96 real-time PCR
7 machine using the following primers; β-Actin: F AGCACTGTGTTGGCGTACAG, R
8 AGAGCTACGAGCTGCCTGAC, PSMB4: F GATCCGGCGTCTGCACTTACAG, R
9 CATGTCTGCGGCAATCACCACTC, TOPORS: F GACACCGACCTAGCTTCTGGG, R
10 TTTGCTAGTGCCAGCTTAGGTG. Relative mRNA expression levels of *TOPORS* was
11 normalized to either β-Actin or PSMB4 using the $2^{-\Delta\Delta C_t}$ method.

12

13 **End-specific qPCR for HpaII-digestable LINE-1 promoters**

14 The LINE-1 end-specific qPCR (ESPCR) to quantify demethylated LINE-1 promoters was
15 performed as previously described⁷² with minor modifications. Primers, facilitator
16 oligonucleotides (Foligos), and probes were synthesized according to the published
17 sequences⁷², except for the HpaII-cut specific reverse Foligo: 5'-
18 TGGCTGTGGGTGGTGGGCCTCGTAGAGGCCCTTTGGTCGGTACCTCAGATGG
19 AAATGTCTT/3ddC/-3'. For a 20 μL reaction, 10 μL of master mix was added to 10 μL of
20 DNA. The master mix composition included 4.0 μL of 5X ESPCR buffer, 1.2 μL of 50 mM
21 MgCl₂, 1.0 μL of 20× DraI-cut specific oligonucleotide mixture, 1.0 μL of 20× HpaII-cut
22 specific oligonucleotide mixture, 0.2 μL of HpaII enzyme (NEB, #R0171L), 0.05 μL of DraI
23 enzyme (NEB, #R0129L), 0.1 μL of Hot Start Taq DNA Polymerase (NEB, #M0495L), and
24 2.45 μL of nuclease-free water. qPCR was conducted using a BioRad CFX96 real-time PCR
25 machine under the following conditions: 37°C for 15 min; 90°C for 5 s; 95°C for 2 min; then

1 10 cycles of 90°C for 5 s, 95°C for 15 s, 60°C for 1 min, and 68°C for 20 s; followed by 40
2 cycles of 95°C for 15 s, 65°C for 40 s, and 68°C for 20 s. FAM and HEX readings were
3 recorded at 65°C during the final stage of 40 cycles. The efficiency of the FAM and HEX
4 reactions was calculated using a standard curve generated from 4 pg to 4 ng of DNA from
5 AZA-treated RKO cells. The relative demethylation of LINE-1 promoters in samples was
6 calculated using $\Delta\Delta C_T$, normalised to the average vehicle $\Delta\Delta C_T$.

7

8 **Western Blotting**

9 Nuclei protein from MOLM-13-Cas9 cells transduced with either sgROSA or sgTOPORS-1
10 treated with 2 doses of DAC or vehicle over 24hrs was extracted in RIPA buffer
11 supplemented with protease inhibitor (Roche, #04693159001). 10ug of protein was boiled in
12 NuPAGE LDS sample buffer (Invitrogen, #NP0007) containing 0.1M DTT and samples run
13 on 4-12% Bis-Tris gel. (Invitrogen, #NP0323) and transferred to PVDF (Thermofisher
14 Scientific, # 88518). Blocked membranes were probed overnight at 4°C with primary
15 antibodies diluted 1:1000 in 5% skim milk in TBST. Primary antibodies used were: anti-
16 DNMT1(Cell Signaling Technology #5032) or anti-SUMO-2/3 (MBL Life Science #M114-
17 3). Membranes were stripped in 15g glycine, 1g SDS, 10ml Tween-20, pH2.2 then re-probed
18 with re-probed with anti- β actin (Santa Cruz Biotechnology, #sc-47778). HRP-conjugated
19 anti-rabbit and anti-mouse secondary antibodies (Dako #P0448 and #P0260) were diluted
20 1:2000 and incubated for one hour at room temperature. Chemiluminescent signal was
21 detected using Clarity Western ECL Substrate (Biorad, #1705061) and visualised using the
22 iBright CL1500 Imaging System (Invitrogen).

23

24 **AZA-MS**

1 AZA-MS was used to measure levels of 5 aza-dC and 5 me-dC in genomic DNA as
2 previously described³⁸.

3

4 **Nuclear Proteomics**

5 Nuclear lysates were prepared by resuspending cell pellets in lysis buffer (10mM Tris pH 8.0,
6 10mM NaCl, 0.2% NP40) supplemented with protease inhibitors (Roche, # 4693159001) and
7 phosSTOP (Roche, # 4906837001), incubating for 10 min on ice, and pelleting nuclei at
8 1450g. The nuclear pellet was lysed in ice-cold RIPA (50mM TrisHCl pH7.5, 150mM NaCl,
9 1% Triton X-100, 0.5% Deoxycholic acid, 0.1% SDS) supplemented with protease inhibitors
10 and phosSTOP, with Benzonase added to a final concentration of 50units/mL. Lysates were
11 sonicated on the Bioruptor (Diagenode) at 30s on and 30s off for a total of 3 cycles and
12 incubated on ice for 15 minutes. Samples were spun down at 8000 x g for 15 minutes at 4°C
13 and the protein supernatant was collected into a fresh tube. Quantified nuclear protein lysate
14 was used for mass spectrometry-based label-free protein quantification as described⁷³.

15

16 LC-MS/MS raw files were pre-processed and analyzed using the MaxQuant software
17 suite (Version 1.6.2.10.43) for feature detection, protein identification and quantification, and
18 sequence database searches were performed using the integrated Andromeda search engine as
19 previously described⁷³ . MaxQuant pre-processed files were loaded into LFQ-Analyst⁷⁴ for
20 label-free protein quantification using cutoffs of FDR< 0.05, |Log₂Fold-Change|>1, with a
21 perseus-type imputation, Benjamini Hochberg FDR correction, and inclusion of single
22 peptide identifications.

23

24 **LC-MS/MS of Ni-NTA enrichment of 10His-SUMO1ylated proteins**

1 A human codon optimised sequence encoding HHHHHHHHHH-
2 MSDQEAQPSTEDL GDKKEGEYIKLK VIGQDSSEIHF KV KMTTHLKKL KESYCQRQG
3 VPMNSLRFLFEGQRIADNHTPKELGMEEEDVIEVYQEQTGG (10His-SUMO1) was
4 fused to DasherGFP separated by the T2A peptide EGRGSLLT CGDVEENPGP and cloned
5 into lentiviral vector pD2109-EF1 by Atum Bio (Fig. S6A), and lentiviral particles used to
6 stably transduce gene-edited MOLM-13 cells. DasherGFP⁺tagRFP⁺ gene-edited MOLM-13
7 cells purified by FACS were cultured in quadruplicate and treated with 41nM DAC or vehicle
8 daily for 3 days. 10His-SUMO1ylated proteins were enriched from 6M guanidine whole cell
9 extracts using Ni-NTA beads following the detailed procedure of⁵⁴, stopping the enrichment
10 process at Step 47. Proteomic data was recovered from the enriched proteins using LC-MS/MS
11 of trypsin digests as for nuclear proteins from gene edited MDS-L cells.

12

13 **Xenotransplantation into MISTRG mice**

14 MISTRG mice³³ were bred and maintained in SPF conditions in HEPA filtered cages at \leq 5
15 mice per cage under protocols approved by the Animal Care and Ethics Committee of the
16 University of New South Wales.

17 **Cord blood CD34+ cells:** MISTRG neonates (2–3 days old) were xeno-transplanted by
18 intrahepatic injection with 2000–3000 CD34+ human cord blood cells in 25 μ L neutral saline
19 as described³³, with the omission of neonatal irradiation. Engraftment levels were quantified
20 by flow cytometry of tail bleeds performed no earlier than 7 weeks of age and expressed as
21 the percentage of human CD45+ (huCD45+) cells to total huCD45+ plus mouse CD45+
22 (moCD45+) cells in the tissue sample. To randomly distribute treatments across cages, mice
23 were rank randomized according to sex and %huCD45+ in cohorts equal to the number of
24 treatment groups prior to commencement of drug treatments, which then proceeded as
25 described in the Figures.

1 **MOLM-13 cells:** Warmed adult MISTRG were tail vein injected with 5×10^4 (females) or 10^5
2 (males) luciferase⁺ MOLM-13 cells i.v. in an inoculum of 0.1mL neutral saline. Injected mice
3 were maintained with a constant supply of sterile filtered 0.27mg/mL enrofloxacin (Bayer)
4 antibiotic in their drinking water. Engraftment was first assessed about 10 days after
5 inoculation using an IVIS SpectrumCT Preclinical In Vivo Imaging System (PerkinElmer)
6 for whole body luminescence imaging under isoflurane anaesthesia, as described⁷⁵. Mice
7 were then rank randomized according to sex and pre-treatment luminescence flux in cohorts
8 equal to the number of treatment groups prior to commencement of drug treatments.

9 **Primary AML cells:** The origin and maintenance of patient AML-5 cells as continuous
10 mouse xenografts in NSG strain mice is described⁵⁶. Freshly thawed AML-5 xenograft mouse
11 bone marrow and spleen cells (>95% huCD45+) were injected into 8 week old MISTRG
12 males and females (1.25×10^6 cells per mouse) that had received 250 cGy sub-lethal
13 irradiation 24h prior. Xeno-engrafted mice were ranked randomized according to sex and
14 weight in cohorts equal to the number of treatment groups. Drug treatment cycles then
15 commenced 11 days after inoculation and proceeded as described in Figures. Engraftment
16 levels were quantified by flow cytometry of tail bleeds as above, sampled at ~1 week
17 intervals.

18 **Xenograft drug treatments:** HMA stocks (30mg/mL for AZA; 10mg/mL for DAC)
19 dissolved in anhydrous DMSO and stored at -80C under argon in small aliquots were diluted
20 into neutral saline immediately before use and administered i.p. or s.c. at the concentrations
21 specified in a bolus of 5mL/kg. TAK-981 prepared as a 4-5mg/mL working solution in 20%
22 hydroxypropyl β -cyclo-dextrin vehicle (HPBCD; Onbio Inc.) at pH 3.5–4 (stored at -80C for
23 ≤ 8 weeks), was diluted in HPBCD vehicle if necessary and injected i.p. at 5mL/kg.
24 Tetrahydouridine (THU, Abcam) dissolved to 2mg/mL in neutral saline (stored at -20C for
25 ≤ 12 weeks) was injected i.p. at 5mL/kg.

1

2 **Data Availability**

3 Data from the CRISPR dropout screen and RNA sequencing have been deposited at GEO
4 under accession #GSE261339. The mass spectrometry proteomics data have been deposited
5 to the ProteomeXchange Consortium with the dataset identifier PXD050539.

1 ACKNOWLEDGMENTS

2 The authors thank the staff and donors of the Sydney Cord Blood Bank for providing cord
3 bloods for research, Takeda Pharmeceuticals for provision of TAK-981 for use in mice, Prof
4 Kaylene Simpson (Peter MacCallum Cancer Centre) for provision and advice with the
5 CRISPR lentiviral library, Forrest Koch (UNSW) for assistance with genotyping, Dr Ivo A.
6 Hendriks (University of Copenhagen) for advice on SUMO pulldown assays, Dr Antony
7 Rongvaux (Fred Hutchinson Cancer Research Centre) for advice on MISTRG colony
8 maintenance and xenotransplantation, Dr Gil Prive and Dr. Brian Raught (University of
9 Toronto) for stimulating discussions. Some of the data presented in this work were acquired
10 by personnel and/or instruments of the National Imaging Facility, a National Collaborative
11 Research Infrastructure Strategy (NCRIS) capability, at the Mark Wainwright Analytical
12 Centre (MWAC) of UNSW Sydney, which is funded in part by the Research Infrastructure
13 Programme of UNSW. The Victorian Centre for Functional Genomics is funded by the
14 Australian Cancer Research Foundation, Phenomics Australia through funding from the
15 Australian Government's National Collaborative Research Infrastructure Strategy program,
16 and the Peter MacCallum Cancer Centre Foundation. This work was supported by
17 Postgraduate Awards from UNSW Sydney (P.T, A.A, X.Z, G.S.B, E.G) and Translational
18 Cancer Research Network-a Translational Cancer Research Centre funded by the Cancer
19 Institute NSW (P.T.); the Anthony Rothe Memorial Trust (J.T, J.E.P, P.C); Cancer Council
20 NSW (RG 23-08, P.C), Ideas Grant from the National Health and Medical Research Council
21 of Australia (GNT2011627; C.J.J, J.E.P); Research Fellowship from the National Health and
22 Medical Research Council of Australia (APP1157871; R.B.L.); program grants from the
23 Leukemia Lymphoma Society (LLS)-Snowdome Foundation-Leukaemia Foundation (6620-
24 21; J.E.P), Cancer Institute NSW (TPG2152; J.E.P, J.T) and Medical Research Future Fund

1 (MRF1200271; J.E.P). Children's Cancer Institute Australia is affiliated with UNSW Sydney
2 and The Sydney Children's Hospitals Network.

1 AUTHOR CONTRIBUTIONS

2 P.T, S.S, S.J, Md. I. I, L. Z, M.J.R, A.A, M.N, X.Z, G.S.B, C.H.S, E.G, O.S, S.M, C.E.T,
3 P.C, P.M.K, S.K.B, K.A.M, J.A.I.T, C.J.J performed the research and analyzed the data;
4 M.R, H. A-R, J.L, P.C., K.A.M, R.B.L and C.W provided key reagents, discussed, and
5 interpreted the data. The study was conceived by J.E.P. The manuscript was written by P.T.
6 and C.J.J with contributions from J.A.I.T and J.E.P.

7

8

1 COMPETING INTERESTS

2 P.T, J.A.I.T, C.J, and J.P are listed as inventors/contributors in P0054922PCT. The remaining
3 authors declare no competing financial interests.

4

5

1 **FIGURE LEGENDS**

2 **Figure 1. Genome-wide CRISPR-Cas9 dropout screening identifies novel genetic**
3 **determinants of AZA-sensitivity.** (A) Schematic of the genome-wide CRISPR-Cas9
4 dropout screen workflow performed in AZA-treated Cas9-expressing MDS-L. Image made
5 with BioRender. (B) MAGeCKFlute nine-square correlation plot using cell-cycle normalized
6 β scores calculated for each gene target (n=2). Colors: sgRNAs specifically (●) enriched, or
7 (●) depleted under AZA selection. (C) ClueGO pathway term network highlighting
8 biological processes enriched in dropout hits. (D) Competitive proliferation assay workflow.
9 MDS-L/Cas9 cells were transduced with lentiviral vectors encoding a single sgRNA plus a
10 tagRFP657 (tagRFP657) reporter from separate promoters. Image made with BioRender. (E)
11 Validation of AZA-selection against *TOPORS*-, *UBE2K*-, and *UBXN7*-editing using the
12 competitive proliferation assay shown in D. In each plot, y = %tagRFP⁺ in AZA/mean
13 %tagRFP⁺ in vehicle; n=3.

14

15 **Figure 2. Loss of TOPORS sensitizes MDS and AML cell lines to AZA.** (A-B) Dose-
16 survival plots of tagRFP⁺ cell counts following four daily applications of AZA MDS-L cells
17 polyclonally expressing Cas9 plus (A) single sgRNAs, or (B) single shRNAs which targeted
18 *TOPORS* or a non-targeting control. Dots are means (n=4) normalized to the vehicle control,
19 \pm SD. P-value is from an extra sum-of-squares F test. (C) Clonogenic assays performed using
20 *TOPORS*-edited MDS-L cells pre-treated with 0.3 μ M AZA as in A before plating in
21 methylcellulose medium. Colonies were counted two weeks after methylcellulose plating. 2-
22 way ANOVA: *** P \leq 0.001, **** P \leq 0.0001. (D) Dose-survival plots of tagRFP⁺ cell
23 counts following 4 days of daily treatment with the indicated AZA concentrations in AML
24 cell lines polyclonally expressing Cas9 plus single sgRNAs or a non-targeting control
25 sgRNA. Dots are means (n=4) normalized to the vehicle control, \pm SD. P-values are from

1 extra sum-of-squares F tests. (E) The change in whole body luminescence flux in MISTRG
2 mice engrafted with 10^5 MOLM-13 cells which polyclonally express luciferase, Cas9 and the
3 indicated sgRNAs, immediately following 1 cycle of treatment with AZA or vehicle i.p.- as
4 described by the time-based x-axis in F. FDR q-values (threshold = 0.01) are reported for a
5 Mann-Whitney multiple comparison test; n=7–10. (F) Kaplan-Meier plots for survival of the
6 same MISTRG mice as E. Whole body luminescence (“IVIS”) was performed 8 days after
7 engraftment to give a “pre-AZA” baseline (which was used to rank-randomize mice into
8 treatment groups based on sex and relative engraftment- “pre-AZA” in E), and again on day
9 18 – two days after completion of the treatment cycle (“post-AZA” in E). Event-free survival
10 was scored according to ethics guidelines. ** Mantel-Cox test P=0.0029 for sgCONTROL
11 versus sgTOPORS-2 at 1.0mg/kg AZA.

12

13 **Figure 3. Targeting TOPORS functionally spares healthy hematopoiesis.** (A) Workflow
14 for lentiviral stable sgRNA + tagRFP delivery, followed by electroporation of transient Cas9-
15 GFP fusion mRNA into primary CD34⁺ cord blood-derived HSPCs for target gene editing.
16 Image made with BioRender. (B) Colony forming capacity of tagRFP-sorted gene-edited
17 CD34⁺ HSPCs pre-treated with AZA. Data are mean and range; n = 2 experiments using
18 independent cord blood donors. (C) Workflow for engraftment into MISTRG neonates with
19 tagRFP-sorted gene-edited CD34⁺ HSPCs, followed by drug-treatment, blood monitoring,
20 and endpoint analysis of the engrafted adults. Image made with BioRender. (D) Tracking of
21 tagRFP⁺-frequencies in huCD45⁺moCD45⁻ cells for each engrafted mouse indicating
22 frequencies (circles) before drug treatment, (diamonds) after one AZA cycle, and (squares)
23 after AZA followed by DAC cycles. Bars indicate means for each treatment group (n = 5 per
24 group). (E-F) Endpoint bone marrow frequencies for each engrafted mouse, with line for
25 mean; (E) % tagRFP⁺ cells amongst huCD45⁺moCD45⁻ cells, or (F) % CD34⁺ tagRFP⁺

1 huCD45⁺ moCD45⁻ cells amongst all CD45⁺ cells. (G) Polyclonal indel KO scores generated
2 by ICE algorithm for tagRFP⁺CD34⁺huCD45⁺moCD45⁻ cells sorted from endpoint bone
3 marrows. Bars: means \pm SD. Dashed line: Polyclonal indel KO score generated by ICE
4 algorithm for day of engraftment.

5

6 **Figure 4. Targeting TOPORS sensitizes leukemic cells to HMAs via defective DDR.** (A)
7 Mean fluorescence intensity of anti- γ H2AX staining by FACS of fixed/permeabilized gene-
8 edited MDS-L cells treated daily with 0.3 μ M AZA for 4 days. ** P < 0.01 compared to every
9 other treatment by one-way ANOVA, n = 3; P > 0.05 comparisons not shown. Inset: FACS
10 data representing the middle data point for each treatment. (B) Detection of DNA breaks by
11 comet assay in gene-edited MDS-L cells treated with 0.3 μ M AZA as for A. **** P \leq 0.0001,
12 for Kruskal-Wallis multiple comparison tests, n = 75; P > 0.05 are not shown. (C) Example
13 DNA content profiles determined by DAPI staining of gene-edited MDS-L cells treated with
14 0.3 μ M AZA. (D) Stacked histograms from biological triplicates of C; *** P < 0.001
15 compared to every other treatment by two-way ANOVA; P > 0.05 comparisons not shown.
16 (E) Proportion of apoptotic cells determined by Annexin/PI staining in gene-edited MDS-L
17 cells treated with 0.3 μ M AZA . **** P < 0.0001, ** P < 0.01, one-way ANOVA, n = 3; P >
18 0.05 comparisons not shown. (F) Incorporation of 5 aza-dC, and (G) methylation at dC, in
19 genomic DNA (both determined by LC-MS) in gene-edited MDS-L cells exposed to 0.3 μ M
20 AZA or 0.02 μ M DAC daily as for A. ** P \leq 0.01, ns P > 0.05, for selected pairwise
21 comparisons in one-way ANOVA, n = 3.

22

23 **Figure 5. Multi-omic approaches reveal widespread mis-splicing of DDR genes and cycle**
24 **delay in AZA-treated TOPORS-edited MDS-L cells.** (A) Gene set enrichment analysis of
25 differentially expressed genes using the KEGG module as part of the clusterProfiler

1 algorithm. Dot plots depict gene sets that are enriched or suppressed in AZA-treated
2 *TOPORS*-edited MDS-L cells compared to AZA-treated control cells. GeneRatio refers to the
3 ratio of input genes that are annotated in a term. (B) Transcription factors with targets
4 demonstrating significant overlap with differentially upregulated genes in AZA-treated
5 *TOPORS*-edited MDS-L cells compared to vehicle determined through TRRUST. (C)
6 Unsupervised hierarchical clustering and heatmap of 3826 most significant differentially
7 spliced events between all samples (n=12). Histograms at right show the proportion of mis-
8 spliced events detected as percentage of all splicing events. (D) Number of alterative splicing
9 events detected in AZA-treated *TOPORS*-edited MDS-L compared to AZA-treated control
10 cells. (E) Overrepresentation analysis of skipped exon events detected in AZA-treated
11 *TOPORS*-edited MDS- L cells compared to AZA-treated control cells. (F) Motif scanning
12 analysis for AGCGGA (SRSF6) binding sites across a meta-exon (green) generated from all
13 exon skipping events. Motif enrichment scores (left axis) and $-\log_{10}(P$ values) (right axis) are
14 shown. (red) Motif enrichment scores of exons differentially retained in AZA-treated
15 *TOPORS*-edited MDS-L cells. (blue) Motif enrichment scores of exons differentially skipped
16 in AZA-treated *TOPORS*-edited MDS-L cells. (dashed) Significance scores. (black)
17 background score calculated from all non-differentially spliced exons.
18

19 **Figure 6. Nuclear proteomics reveals a depletion of global nucleotide excision repair**
20 **factors in AZA-treated *TOPORS*-edited MDS-L cells.** (A) Heatmap of unsupervised
21 hierarchical clustering of 73 proteins that were significantly differentially abundant across all
22 nuclear extracts from triplicate cultures of gene-edited MDS-L cells treated daily with 0.3 μ M
23 AZA or vehicle for 4 days; n = 12. (B) Overrepresentation pathway analysis of proteins
24 enriched or depleted in (top) cluster 4 and (bottom) cluster 6. (middle) Normalized total
25 spectra (Scaffold 5.3.2) for DNMT1 peptides detected in each replicate. **** P < 0.0001, ***

1 P < 0.001, ** P < 0.01, one-way ANOVA, n = 3; P > 0.05 comparisons not shown. (C)
2 Sequential detection in the same western blot of (top) DNMT1, then (middle) β -actin, then
3 (bottom) SUMO2/3 in 10 μ g nuclear proteins from gene-edited MOLM-13 cells treated with
4 42nM DAC or vehicle daily in triplicates for 3 days.

5

6 **Figure 7. TOPORS-editing sensitizes cells to HMA in a DNMT1-dependent manner.** (A)
7 (left axis) Survival of gene-edited or wild-type MDS-L cells in 96-well plates in response to
8 daily doses of DNMTi GSK3685032 or vehicle on days 1–4. (left axis) tagRFP+ cells (or all
9 cells for wild-type MDS-L) were counted on day 5 and normalized to vehicle counts. (right
10 axis) In a separate experiment, relative demethylation of LINE-1 promoters in wild-type
11 MDS-L was determined (see Methods) for a similar GSK3685032 dose range and normalized
12 to vehicle control cells. (B) Gene-edited MDS-L cells were plated into 96-well plates and
13 treated with 1 μ M GSK3685032 or vehicle on day 1. Varying DAC plus 1 μ M GSK3685032
14 or vehicle was added daily on days 2–4, and tagRFP+ cells counted on day 5, and normalized
15 to vehicle counts. (C–D) Gene-edited MDS-L cells were plated into 96-well plates and treated
16 day 1 only with (C) Topotecan or (D) Etoposide or vehicle. tagRFP+ cells were counted on
17 day 5 and normalized to vehicle counts. (E) Gene-edited MDS-L cells in 96-well plates were
18 treated with daily Hydroxyurea or vehicle on days 1–4. tagRFP+ cells were counted on the
19 day 5 and normalized to vehicle counts. In all panels, dots represent mean \pm SD, (A–B) n = 3,
20 (C–E) n = 4. EC50 values deduced from all panels are shown in Table S3.

21

22 **Figure 8. TOPORS-editing does not reduce SUMOylation of DNMT1 in HMA-treated**
23 **AML cells.** Proteomic analysis of whole cell Ni-NTA enriched proteins from gene-edited
24 MOLM-13 cells expressing 10xHis-SUMO1 that were exposed to 42 nM DAC or vehicle for
25 3 days. (A–B) Volcano plots (Scaffold 5.3.2) highlighting proteins significantly more than 2-

1 fold enriched in *TOPORS*-edited cells compared to control cells under (A) “steady-state” (i.e.
2 vehicle treated) conditions or (B) after exposure to DAC. (C) Normalized total spectra
3 (Scaffold 5.3.2) for (left) *TOPORS* or (right) DNMT1 peptides in each replicate. **** P <
4 0.0001, *** P < 0.001, ** P < 0.01, by (TOPORS) one-way ANOVA or (DNMT1) t-test; P >
5 0.05 comparisons not shown. (D) Summary of enrichment into GO Biological pathways for
6 Ni-NTA captured proteins that were differentially abundant between *TOPORS*-edited versus
7 control cells for (top) vehicle-treated or (bottom) DAC-treated conditions.

8

9 **Figure 9. SUMOylation blockade synergizes with HMAs in MDS and AML.** (A)
10 Summary of ZIP synergy scores (\pm 95% CI) for combinatorial drug testing in MDS-L and
11 AML lines determined by SynergyFinder. (B-C) Survival of gene-edited MDS-L cells in 96-
12 well plates in response to (B) AZA \pm 0.1 μ M TAK-981 or (C) DAC \pm 0.1 μ M TAK-981 added
13 daily on days 1–4. TagRFP+ cells were counted on day 5, and normalized to vehicle counts
14 \pm SD. EC50 values are listed in Table S4. (D) Mean fluorescence intensity of anti- γ H2AX
15 staining by FACS of fixed/permeabilized gene-edited MDS-L cells drug-treated as in B–C.
16 **** P < 0.0001, *** P < 0.001, ** P < 0.01, by one-way ANOVA; P > 0.05 comparisons
17 not shown. (E) Cell cycle distributions \pm SD for the same cultures as D (n=3); **** P <
18 0.0001 by two-way ANOVA; only comparisons between combination and single drugs
19 shown. (F) Event-free survival of non-irradiated MISTRG engrafted i.v. with MOLM-13
20 cells (n = 5–7 per treatment). Mice were sex and IVIS flux rank randomised in cohorts of 4
21 into treatment groups on day 10, then drug treatments (20mg/kg TAK-981 i.p., 0.6mg/kg
22 AZA s.c.) commenced on day 11. ** Gehan-Breslow-Wilcoxon test P < 0.01 for AZA versus
23 any other treatment. (G-J) Sub-lethally irradiated MISTRG mice were injected with 1.25×10^6
24 AML-5 PDX cells i.v.; non-irradiated MISTRG mice were injected with 4×10^6 AML-16
25 PDX cells i.v. PDX-injected mice were then bled at approximately weekly intervals. The

1 mice were randomised in sex and weight ranked cohorts of 4 into treatment groups on day 10
2 or 11, then treated with the drugs (20mg/kg TAK-981 i.p., 0.6mg/kg AZA s.c.) starting day
3 11 or 12. (G,I) Spaghetti plots of blood % huCD45⁺CD33⁺ cells, to track expansion of each
4 (G) AML-5 or (I) AML-16 PDX in xenografted mice. The (G) 25% event threshold or (I) 5%
5 event threshold is indicated. (H and J) Kaplan-Meier plots for event-free survival of the same
6 mice as G and I. Event-free survival was scored as time to reach (H) 25% or (I) 5%
7 engraftment of huCD45⁺CD33⁺ cells in peripheral blood ⁵⁵. *** P < 0.001, ** P < 0.01, by
8 Gehan-Breslow-Wilcoxon test; P > 0.05 comparisons not shown.

9

10

11

1 REFERENCES

- 2 1. Fenaux, P. *et al.* Efficacy of azacitidine compared with that of conventional care
3 regimens in the treatment of higher-risk myelodysplastic syndromes: a randomised,
4 open-label, phase III study. *Lancet Oncol.* **10**, 223–232 (2009).
- 5 2. Prébet, T. *et al.* Outcome of high-risk myelodysplastic syndrome after azacitidine
6 Treatment failure. *J. Clin. Oncol.* **29**, 3322–3327 (2011).
- 7 3. Saunthararajah, Y. *et al.* Evaluation of noncytotoxic DNMT1-depleting therapy in
8 patients with myelodysplastic syndromes. *J. Clin. Invest.* **125**, 1043–1055 (2015).
- 9 4. Steensma, D. P. *et al.* Multicenter study of decitabine administered daily for 5 days
10 every 4 weeks to adults with myelodysplastic syndromes: The alternative dosing for
11 outpatient treatment (ADOPT) trial. *J. Clin. Oncol.* **27**, 3842–3848 (2009).
- 12 5. Gu, X. *et al.* Decitabine- and 5-azacytidine resistance emerges from adaptive
13 responses of the pyrimidine metabolism network. *Leuk. 2020* **35**, 1023–1036
14 (2020).
- 15 6. Unnikrishnan, A. *et al.* Integrative Genomics Identifies the Molecular Basis of
16 Resistance to Azacitidine Therapy in Myelodysplastic Syndromes. *Cell Rep.* **20**, 572–
17 585 (2017).
- 18 7. Bogenberger, J. M. *et al.* BCL-2 family proteins as 5-Azacytidine-sensitizing targets
19 and determinants of response in myeloid malignancies. *Leukemia* **28**, 1657–1665
20 (2014).
- 21 8. Yang, H. *et al.* Expression of PD-L1, PD-L2, PD-1 and CTLA4 in myelodysplastic
22 syndromes is enhanced by treatment with hypomethylating agents. **28**, 1280–1288
23 (2013).
- 24 9. Liu, Y.-C. *et al.* Demethylation and Up-Regulation of an Oncogene after
25 Hypomethylating Therapy. *N. Engl. J. Med.* **386**, 1998–2010 (2022).

1 10. Cazzola, M. & Malcovati, L. Myelodysplastic Syndromes — Coping with Ineffective
2 Hematopoiesis. *N. Engl. J. Med.* **352**, 536–538 (2005).

3 11. Lopez, J. S. & Banerji, U. Combine and conquer: challenges for targeted therapy
4 combinations in early phase trials. *Nat. Rev. Clin. Oncol.* **2016** *14*, 57–66 (2016).

5 12. Pollyea, D. A. *et al.* Venetoclax with azacitidine disrupts energy metabolism and
6 targets leukemia stem cells in patients with acute myeloid leukemia. *Nat. Med.* **24**,
7 1859–1866 (2018).

8 13. DiNardo, C. D. *et al.* Venetoclax combined with decitabine or azacitidine in treatment-
9 naive, elderly patients with acute myeloid leukemia. *Blood* **133**, 7–17 (2019).

10 14. DiNardo, C. D. *et al.* Safety and preliminary efficacy of venetoclax with decitabine or
11 azacitidine in elderly patients with previously untreated acute myeloid leukaemia: a
12 non-randomised, open-label, phase 1b study. *Lancet Oncol.* **19**, 216–228 (2018).

13 15. Sallman, D. A. *et al.* Magrolimab in Combination With Azacitidine in Patients With
14 Higher-Risk Myelodysplastic Syndromes: Final Results of a Phase Ib Study. *J. Clin.*
15 *Oncol.* **41**, 2815–2826 (2023).

16 16. Wolff, F., Leisch, M., Greil, R., Risch, A. & Pleyer, L. The double-edged sword of (re
17) expression of genes by hypomethylating agents : from viral mimicry to exploitation
18 as priming agents for targeted immune checkpoint modulation. 1–14 (2017)
19 doi:10.1186/s12964-017-0168-z.

20 17. Chiappinelli, K. B. *et al.* Inhibiting DNA Methylation Causes an Interferon Response
21 in Cancer via dsRNA Including Endogenous Retroviruses. *Cell* **162**, 974–986 (2015).

22 18. Roulois, D. *et al.* DNA-Demethylating Agents Target Colorectal Cancer Cells by
23 Inducing Viral Mimicry by Endogenous Transcripts Article DNA-Demethylating
24 Agents Target Colorectal Cancer Cells by Inducing Viral Mimicry by Endogenous
25 Transcripts. *Cell* **162**, 961–973 (2015).

1 19. Orta, M. L. *et al.* 5-Aza-2'-deoxycytidine causes replication lesions that require
2 Fanconi anemia-dependent homologous recombination for repair. *Nucleic Acids Res.*
3 **41**, 5827–5836 (2013).

4 20. Gruber, E., Franich, R. L., Shortt, J., Johnstone, R. W. & Kats, L. M. Distinct and
5 overlapping mechanisms of resistance to azacytidine and guadecitabine in acute
6 myeloid leukemia. *Leuk. 2020 3412* **34**, 3388–3392 (2020).

7 21. Wang, E. *et al.* Modulation of RNA splicing enhances response to BCL2 inhibition in
8 leukemia. *Cancer Cell* **41**, 164-180.e8 (2023).

9 22. Diesch, J. *et al.* Inhibition of CBP synergizes with the RNA-dependent mechanisms of
10 Azacitidine by limiting protein synthesis. *Nat. Commun.* **2021 121** **12**, 1–13 (2021).

11 23. Rhyasen, G. W. *et al.* An MDS xenograft model utilizing a patient-derived cell line.
12 *Leukemia* **28**, 1142–1145 (2014).

13 24. Makishima, H. *et al.* Dynamics of clonal evolution in myelodysplastic syndromes. *Nat.*
14 *Genet.* **49**, 204–212 (2017).

15 25. Doench, J. G. *et al.* Optimized sgRNA design to maximize activity and minimize off-
16 target effects of CRISPR-Cas9. *Nat. Biotechnol.* **2015 342** **34**, 184–191 (2016).

17 26. Wang, B. *et al.* Integrative analysis of pooled CRISPR genetic screens using
18 MAGeCKFlute. *Nat. Protoc.* **2019 143** **14**, 756–780 (2019).

19 27. Conant, D. *et al.* Inference of CRISPR Edits from Sanger Trace Data. *Cris. J.* **5**, 123–
20 130 (2022).

21 28. Rajendra, R. *et al.* Topors Functions as an E3 Ubiquitin Ligase with Specific E2
22 Enzymes and Ubiquitinates p53. *J. Biol. Chem.* **279**, 36440–36444 (2004).

23 29. Lin, L. *et al.* topors, a p53 and topoisomerase I-binding RING finger protein, is a
24 coactivator of p53 in growth suppression induced by DNA damage. *Oncogene* **2005**
25 **2421** **24**, 3385–3396 (2005).

1 30. Weger, S., Hammer, E. & Heilbronn, R. Topors acts as a SUMO-1 E3 ligase for p53 in
2 vitro and in vivo. *FEBS Lett.* **579**, 5007–5012 (2005).

3 31. Pungaliya, P. *et al.* TOPORS functions as a SUMO-1 E3 ligase for chromatin-
4 modifying proteins. *J. Proteome Res.* **6**, 3918–3923 (2007).

5 32. Weber, K., Bartsch, U., Stocking, C. & Fehse, B. A multicolor panel of novel lentiviral
6 ‘gene ontology’ (LeGO) vectors for functional gene analysis. *Mol. Ther.* **16**, 698–706
7 (2008).

8 33. Song, Y. *et al.* A highly efficient and faithful MDS patient-derived xenotransplantation
9 model for pre-clinical studies. *Nat. Commun.* **10**, 1–14 (2019).

10 34. Yudovich, D. *et al.* Combined lentiviral- and RNA-mediated CRISPR/Cas9 delivery
11 for efficient and traceable gene editing in human hematopoietic stem and progenitor
12 cells. *Sci. Reports 2020 101* **10**, 1–11 (2020).

13 35. Hu, L. Y. *et al.* SUMOylation of XRCC1 activated by poly (ADP-ribosyl)ation
14 regulates DNA repair. *Hum. Mol. Genet.* **27**, 2306–2317 (2018).

15 36. Hariharasudhan, G. *et al.* TOPORS-mediated RAD51 SUMOylation facilitates
16 homologous recombination repair. *Nucleic Acids Res.* **50**, 1501–1516 (2022).

17 37. Renner, F., Moreno, R. & Schmitz, M. L. SUMOylation-Dependent Localization of
18 IKK ϵ in PML Nuclear Bodies Is Essential for Protection against DNA-Damage-
19 Triggered Cell Death. *Mol. Cell* **37**, 503–515 (2010).

20 38. Unnikrishnan, A. *et al.* AZA-MS: A novel multiparameter mass spectrometry method
21 to determine the intracellular dynamics of azacitidine therapy in vivo. *Leukemia* **32**,
22 900–910 (2018).

23 39. Chu, D. *et al.* Cloning and Characterization of LUN, a Novel RING Finger Protein
24 That Is Highly Expressed in Lung and Specifically Binds to a Palindromic Sequence.
25 *J. Biol. Chem.* **276**, 14004–14013 (2001).

1 40. Ji, L. *et al.* TOPORS, a tumor suppressor protein, contributes to the maintenance of
2 higher-order chromatin architecture. *Biochim. Biophys. Acta - Gene Regul. Mech.*
3 **1863**, 194518 (2020).

4 41. Han, H. *et al.* TRRUST: a reference database of human transcriptional regulatory
5 interactions. *Sci. Reports 2015 51* **5**, 1–11 (2015).

6 42. Fouad, S., Hauton, D. & D’Angiolella, V. E2F1: Cause and Consequence of DNA
7 Replication Stress. *Front. Mol. Biosci.* **7**, 435 (2021).

8 43. Choi, E. H. & Kim, K. P. E2F1 facilitates DNA break repair by localizing to break
9 sites and enhancing the expression of homologous recombination factors. *Exp. Mol.*
10 *Med. 2019 519* **51**, 1–12 (2019).

11 44. Agapov, A., Olina, A. & Kulbachinskiy, A. RNA polymerase pausing, stalling and
12 bypass during transcription of damaged DNA: from molecular basis to functional
13 consequences. *Nucleic Acids Res.* **50**, 3018–3041 (2022).

14 45. Jia, N. *et al.* Dealing with transcription-blocking DNA damage: Repair mechanisms,
15 RNA polymerase II processing and human disorders. *DNA Repair (Amst).* **106**, 103192
16 (2021).

17 46. Muñoz, M. J. *et al.* DNA Damage Regulates Alternative Splicing through Inhibition of
18 RNA Polymerase II Elongation. *Cell* **137**, 708–720 (2009).

19 47. Shkreta, L. & Chabot, B. The RNA Splicing Response to DNA Damage. *Biomol.*
20 *2015, Vol. 5, Pages 2935-2977* **5**, 2935–2977 (2015).

21 48. Huttlin, E. L. *et al.* The BioPlex Network: A Systematic Exploration of the Human
22 Interactome. *Cell* **162**, 425–440 (2015).

23 49. Shen, S. *et al.* rMATS: Robust and flexible detection of differential alternative splicing
24 from replicate RNA-Seq data. *Proc. Natl. Acad. Sci. U. S. A.* **111**, E5593–E5601
25 (2014).

1 50. Park, J. W., Jung, S., Rouchka, E. C., Tseng, Y. T. & Xing, Y. rMAPS: RNA map
2 analysis and plotting server for alternative exon regulation. *Nucleic Acids Res.* **44**,
3 W333–W338 (2016).

4 51. Pappalardi, M. B. *et al.* Discovery of a first-in-class reversible DNMT1-selective
5 inhibitor with improved tolerability and efficacy in acute myeloid leukemia. *Nat.*
6 *Cancer* **2021** *210* **2**, 1002–1017 (2021).

7 52. Borgermann, N. *et al.* SUMOylation promotes protective responses to DNA-protein
8 crosslinks. *EMBO J.* **38**, e101496 (2019).

9 53. Liu, J. C. Y. *et al.* Mechanism and function of DNA replication-independent DNA-
10 protein crosslink repair via the SUMO-RNF4 pathway. *EMBO J.* **40**, (2021).

11 54. Hendriks, I. A. & Vertegaal, A. C. O. A high-yield double-purification proteomics
12 strategy for the identification of SUMO sites. *Nat. Protoc.* **2016** *119* **11**, 1630–1649
13 (2016).

14 55. Lightcap, E. S. *et al.* A small-molecule SUMOylation inhibitor activates antitumor
15 immune responses and potentiates immune therapies in preclinical models. *Sci. Transl.*
16 *Med.* **13**, (2021).

17 56. Lee, E. M. *et al.* Efficacy of an Fc-modified anti-CD123 antibody (CSL362) combined
18 with chemotherapy in xenograft models of acute myelogenous leukemia in
19 immunodeficient mice. *Haematologica* **100**, 914–926 (2015).

20 57. Kroonen, J. S. *et al.* Inhibition of SUMOylation enhances DNA hypomethylating drug
21 efficacy to reduce outgrowth of hematopoietic malignancies. *Leuk.* **2023** *374* **37**, 864–
22 876 (2023).

23 58. Gabellier, L. *et al.* SUMOylation inhibitor TAK-981 (subasumstat) synergizes with 5-
24 azacytidine in preclinical models of acute myeloid leukemia. *Haematologica* **109**, 98–
25 114 (2024).

1 59. Marshall, H. *et al.* Deficiency of the dual ubiquitin/SUMO ligase Topors results in
2 genetic instability and an increased rate of malignancy in mice. *BMC Mol. Biol.* **11**, 1–
3 14 (2010).

4 60. Decque, A. *et al.* Sumoylation coordinates the repression of inflammatory and anti-
5 viral gene-expression programs during innate sensing. *Nat. Immunol.* **2015** *17*,
6 140–149 (2015).

7 61. Kazachenka, A. *et al.* Epigenetic therapy of myelodysplastic syndromes connects to
8 cellular differentiation independently of endogenous retroelement derepression.
9 *Genome Med.* **11**, 1–18 (2019).

10 62. Liu, J. C. Y. *et al.* Concerted SUMO-targeted ubiquitin ligase activities of TOPORS
11 and RNF4 are essential for stress management and cell proliferation. *bioRxiv*
12 2023.12.20.572718 (2023) doi:10.1101/2023.12.20.572718.

13 63. Carnie, C. J. *et al.* The dCMP deaminase DCTD and the E3 ligase TOPORS are
14 central mediators of decitabine cytotoxicity. *bioRxiv* 2023.12.21.572728 (2023)
15 doi:10.1101/2023.12.21.572728.

16 64. Wheeler, E. C. *et al.* Splicing modulators impair DNA damage response and induce
17 killing of cohesin-mutant MDS and AML. *Sci. Transl. Med.* **16**, (2024).

18 65. Roboz, G. J. *et al.* Randomized trial of 10 days of decitabine ± bortezomib in untreated
19 older patients with AML: CALGB 11002 (Alliance). *Blood Adv.* **2**, 3608–3617 (2018).

20 66. Ad, L. *et al.* Pevonedistat plus azacitidine vs azacitidine alone in higher-risk
21 MDS/chronic myelomonocytic leukemia or low-blast-percentage AML. *Blood Adv.* **6**,
22 5132–5145 (2022).

23 67. Iskandarani, A. *et al.* Bortezomib-mediated downregulation of S-phase kinase protein-
24 2 (SKP2) causes apoptotic cell death in chronic myelogenous leukemia cells. *J. Transl.*
25 *Med.* **14**, 1–12 (2016).

1 68. Kittai, A. S. *et al.* NEDD8-activating enzyme inhibition induces cell cycle arrest and
2 anaphase catastrophe in malignant T-cells. *Oncotarget* **12**, 2068 (2021).

3 69. Nakamura, A. *et al.* The SUMOylation inhibitor subasumstat potentiates rituximab
4 activity by IFN1-dependent macrophage and NK cell stimulation. *Blood* **139**, 2770–
5 2781 (2022).

6 70. Schnegg-Kaufmann, A. S. *et al.* Contribution of mutant HSC clones to immature and
7 mature cells in MDS and CMML, and variations with AZA therapy. *Blood* **141**, 1316–
8 1321 (2023).

9 71. Joung, J. *et al.* Genome-scale CRISPR-Cas9 knockout and transcriptional activation
10 screening. *Nat. Protoc.* **2017** *12*, 828–863 (2017).

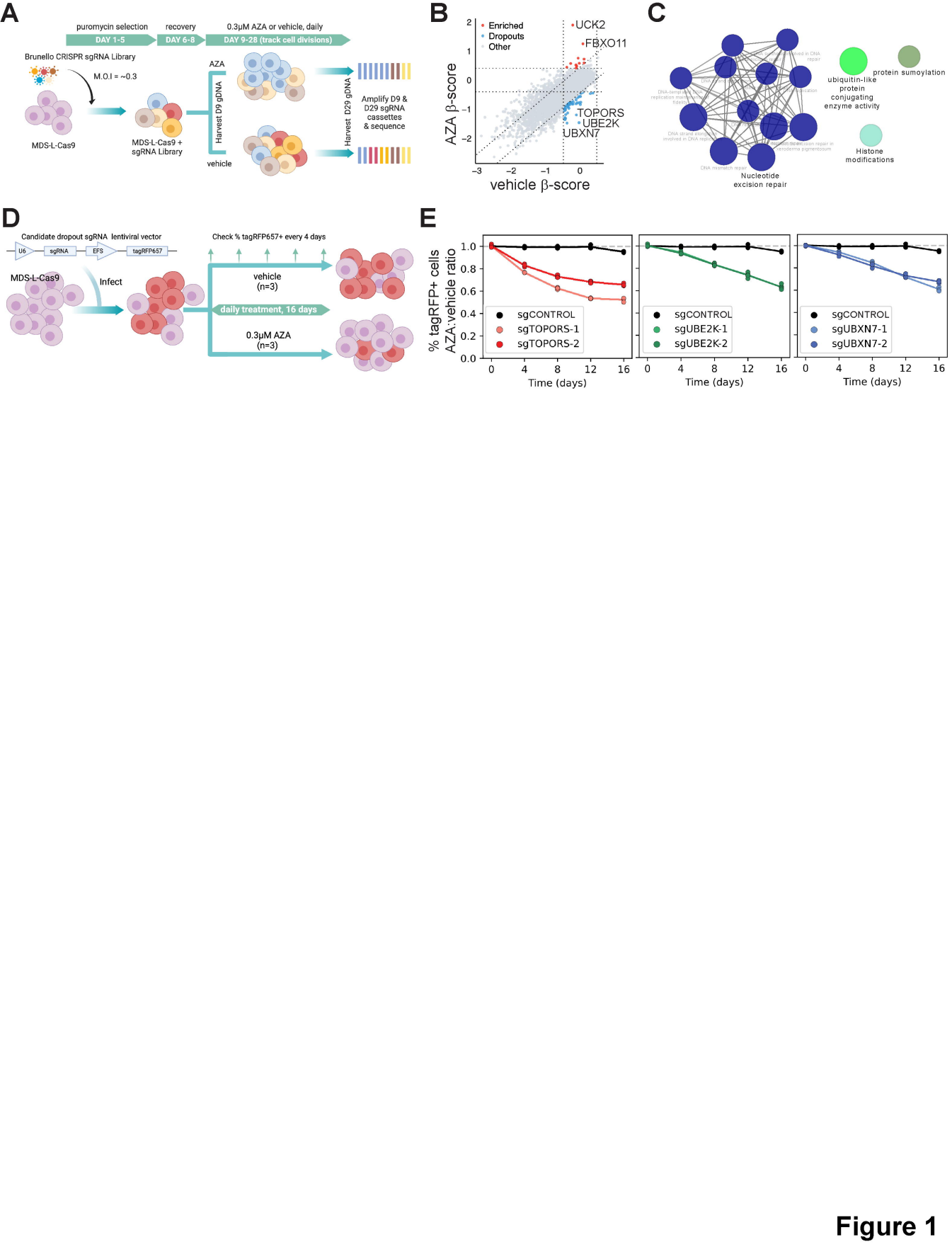
11 72. Rand, K. N. & Molloy, P. L. Sensitive measurement of unmethylated repeat DNA
12 sequences by end-specific PCR. *Biotechniques* **49**, (2010).

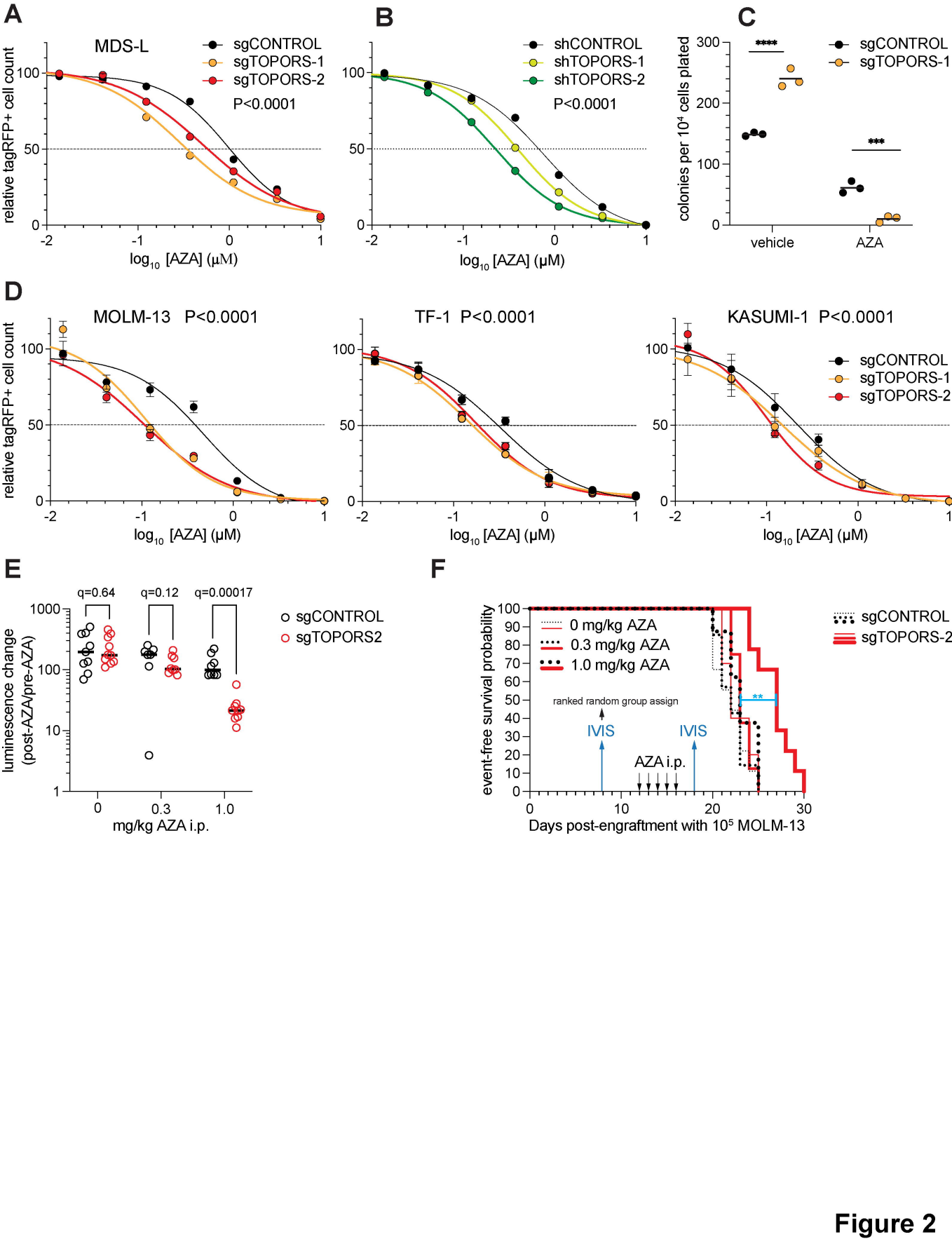
13 73. Awatade, N. T. *et al.* Significant functional differences in differentiated Conditionally
14 Reprogrammed (CRC)- and Feeder-free Dual SMAD inhibited-expanded human nasal
15 epithelial cells. *J. Cyst. Fibros.* **20**, 364–371 (2021).

16 74. Shah, A. D., Goode, R. J. A., Huang, C., Powell, D. R. & Schittenhelm, R. B. Lfq-
17 Analyst: An easy-To-use interactive web platform to analyze and visualize label-free
18 proteomics data preprocessed with maxquant. *J. Proteome Res.* **204**–211 (2019)
19 doi:10.1021/ACS.JPROTEOME.9B00496/SUPPL_FILE/PR9B00496_SI_001.PDF.

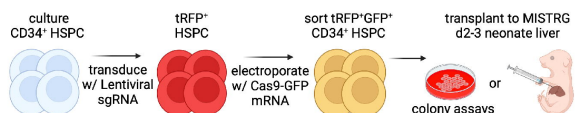
20 75. Jones, L. *et al.* Bioluminescence imaging enhances analysis of drug responses in a
21 patient-derived xenograft model of pediatric ALL. *Clin. Cancer Res.* **23**, 3744–3755
22 (2017).

23

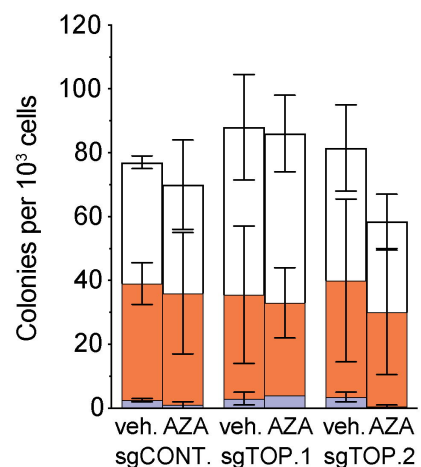




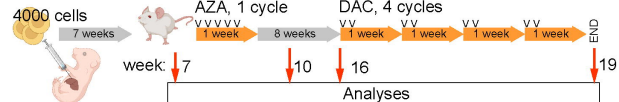
A



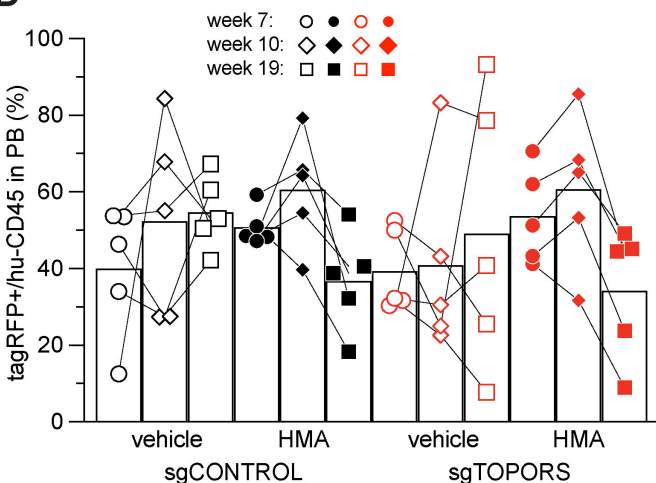
B



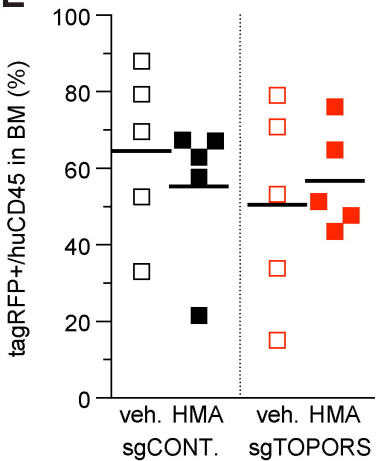
C



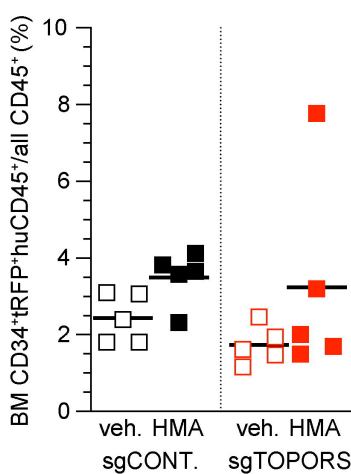
D



E



F



G

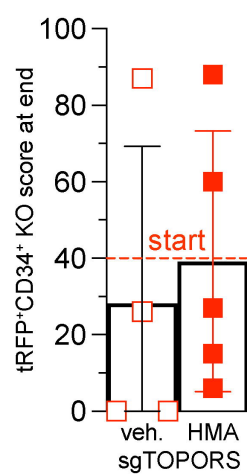


Figure 3

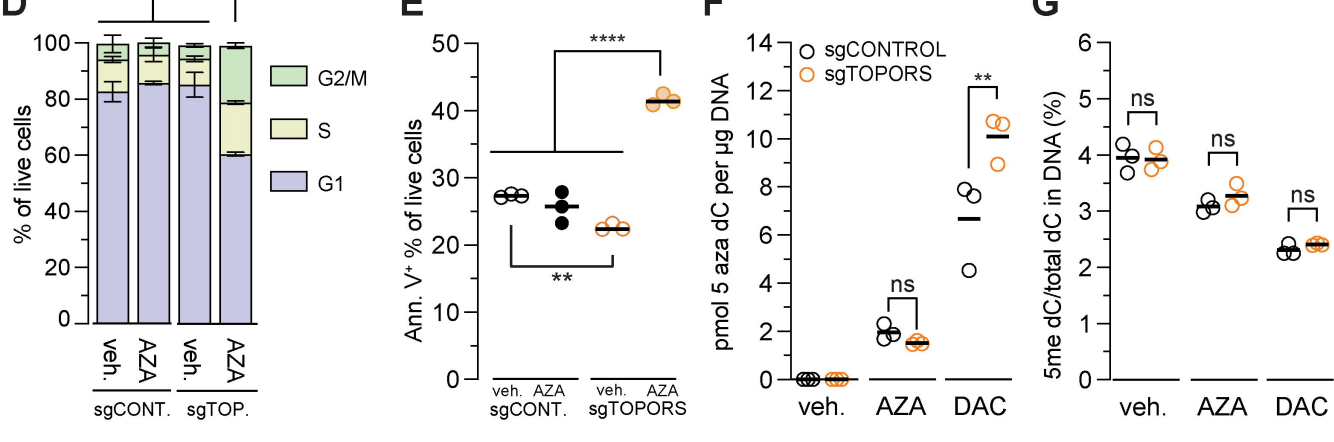
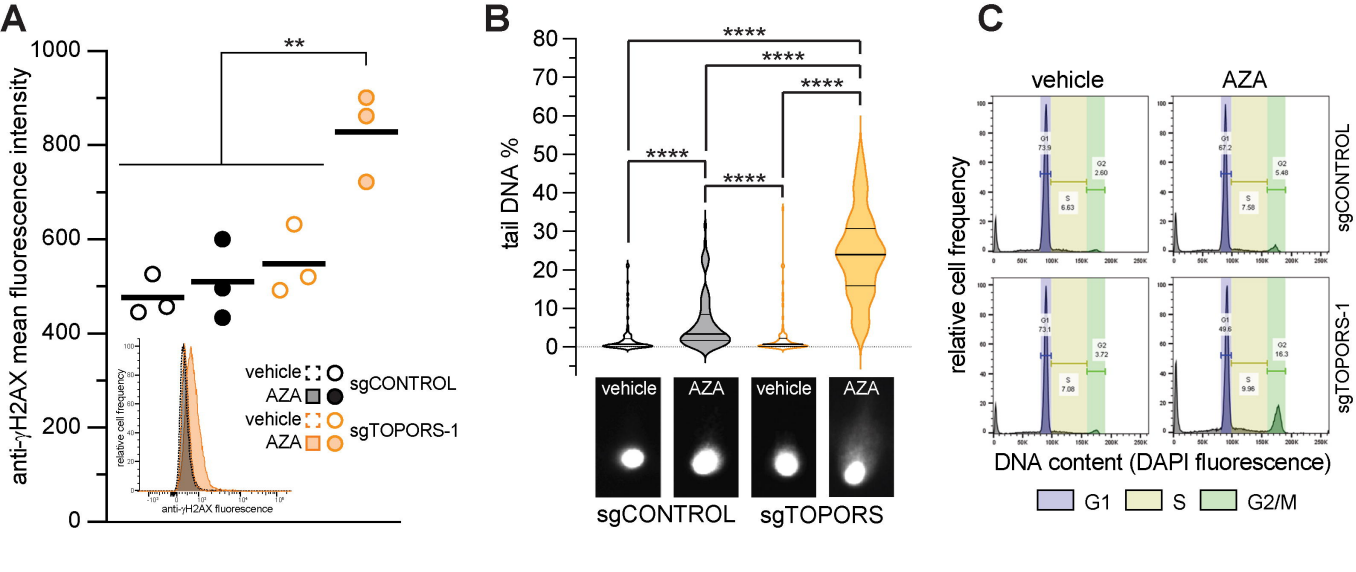
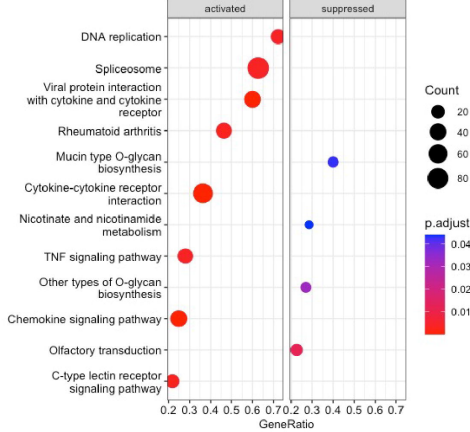


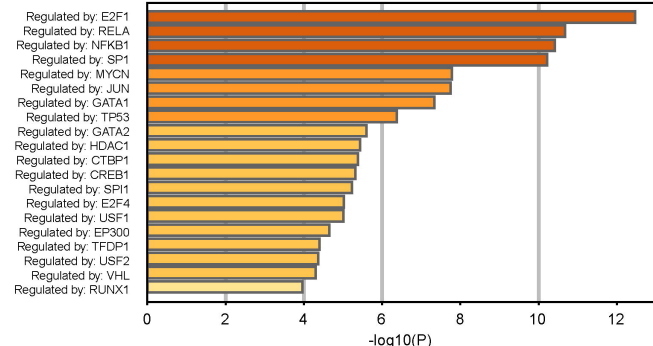
Figure 4

A

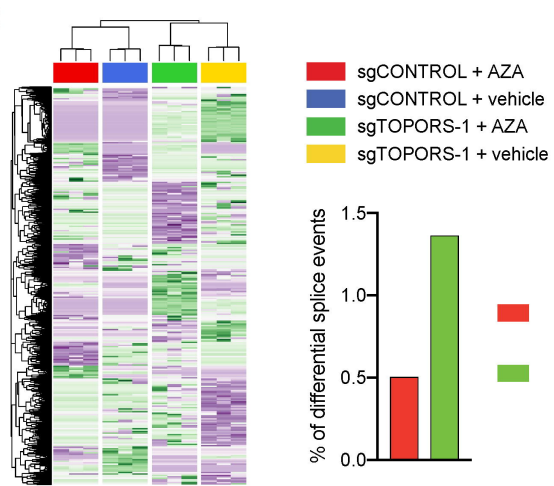
sgTOPORS vs sgCONTROL



B

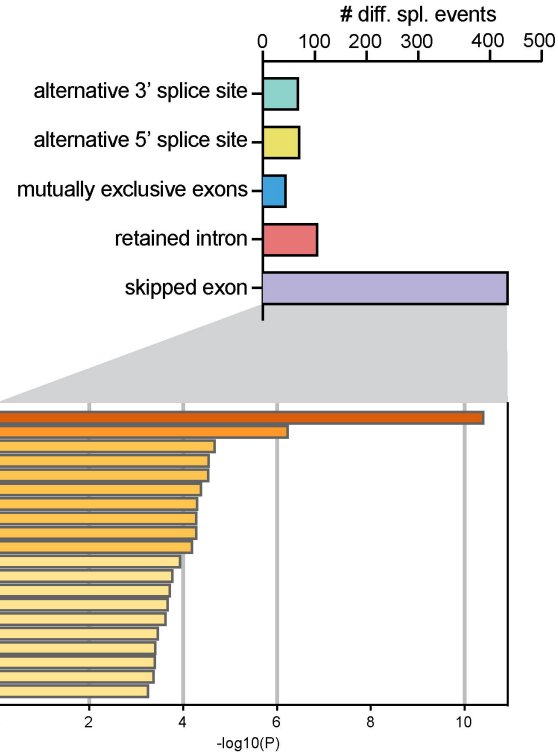


C

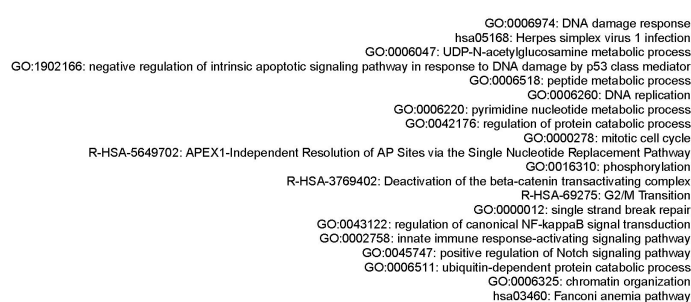


D

sgTOPORS AZA vs sgCONTROL AZA



E



F

Motif MAP: SRSF6-AGCGGA

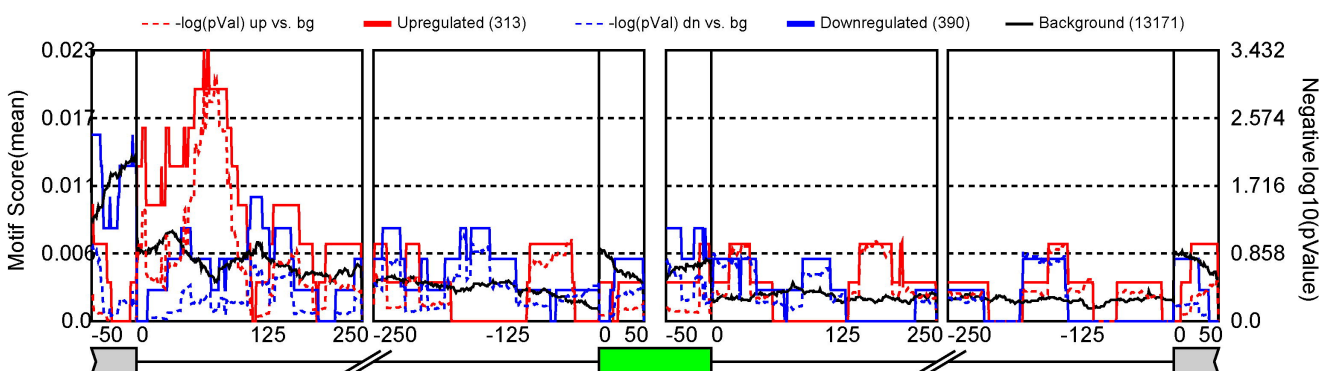


Figure 5

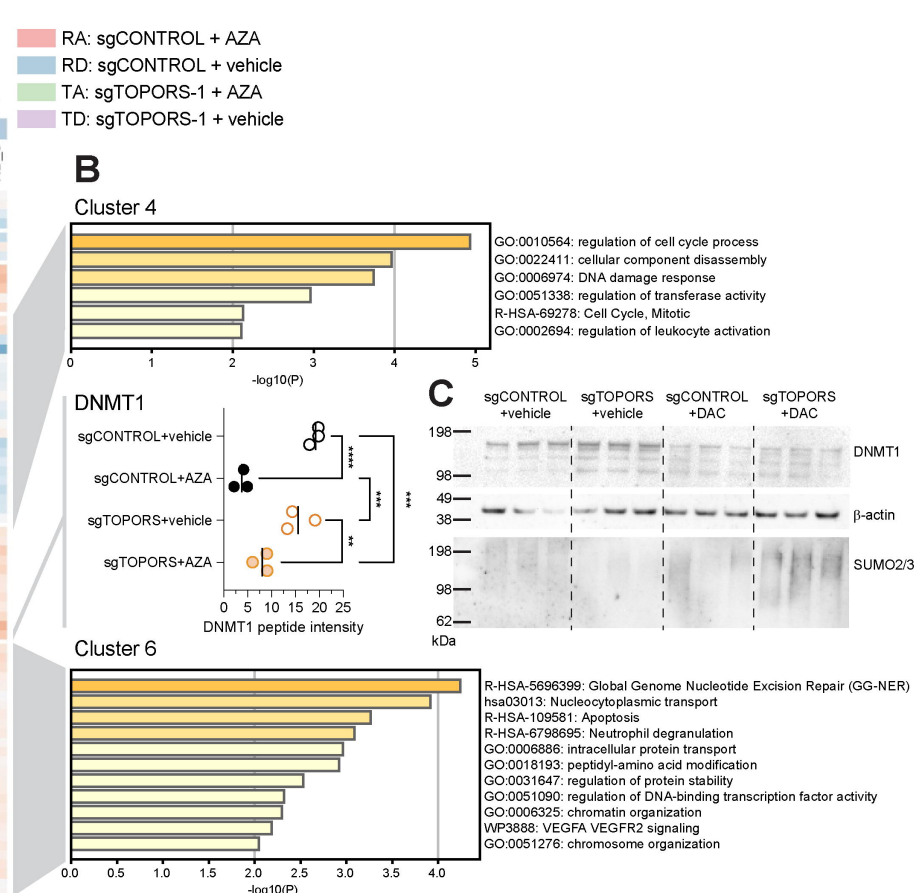
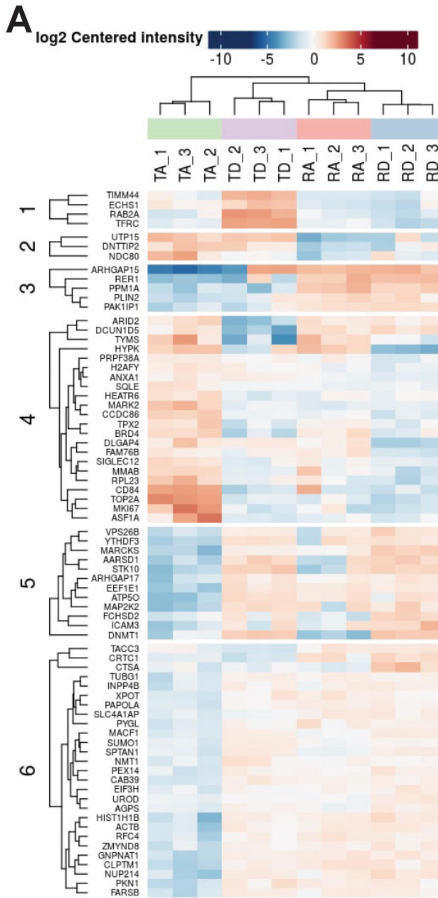
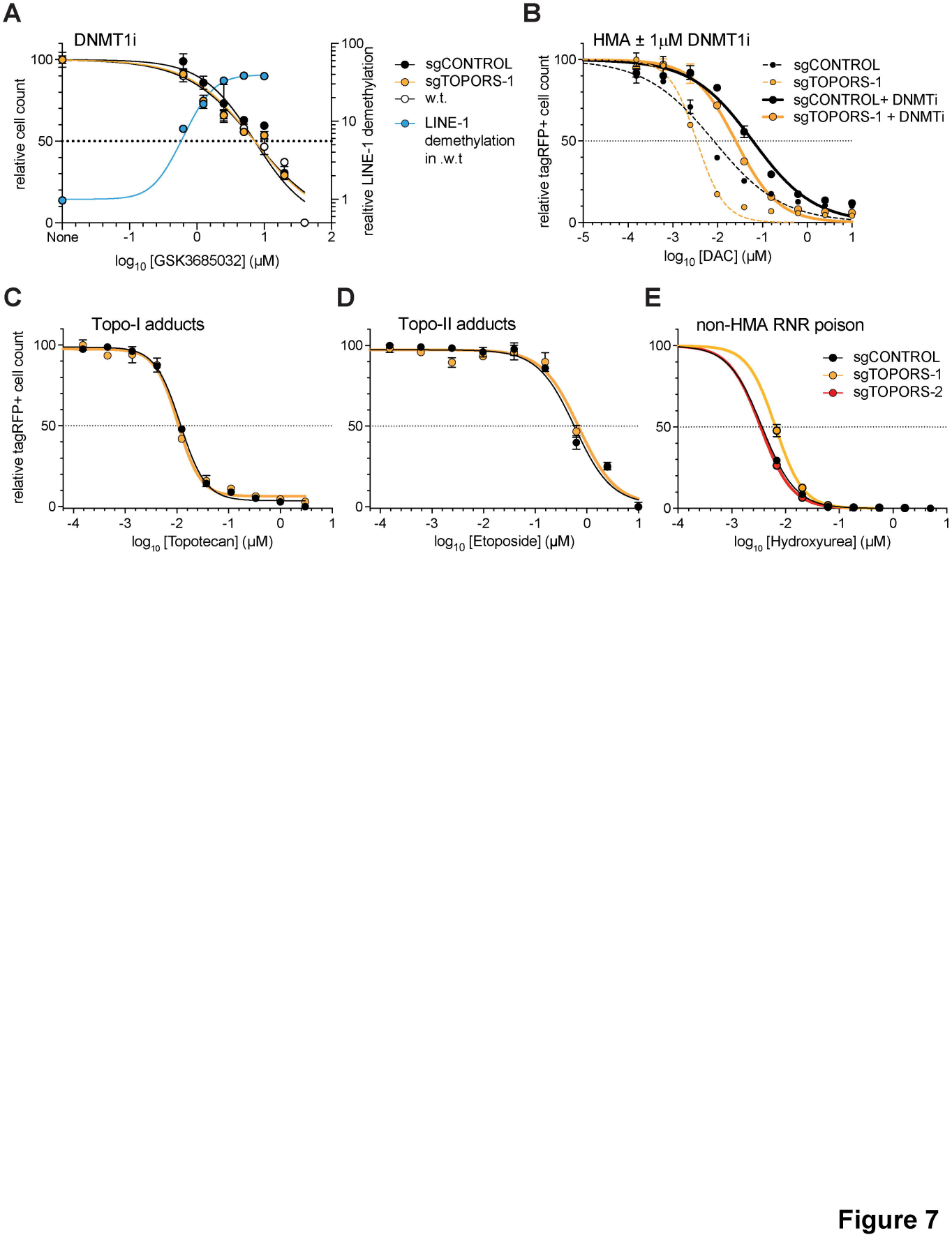


Figure 6



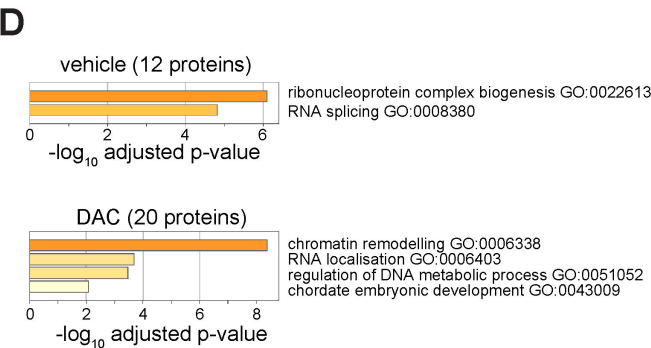
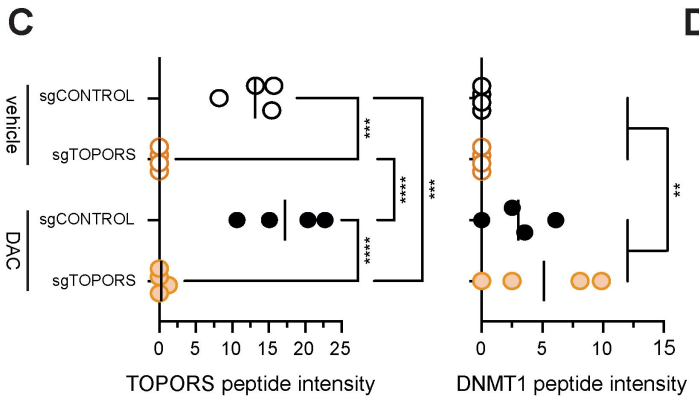
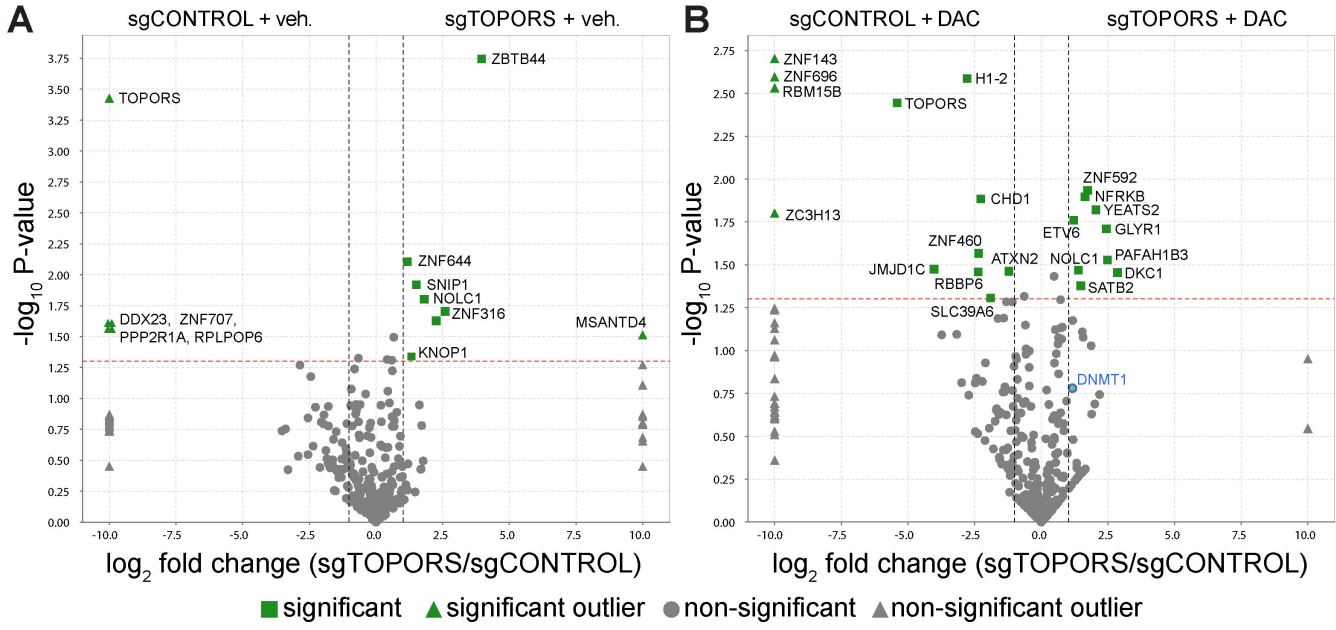


Figure 8

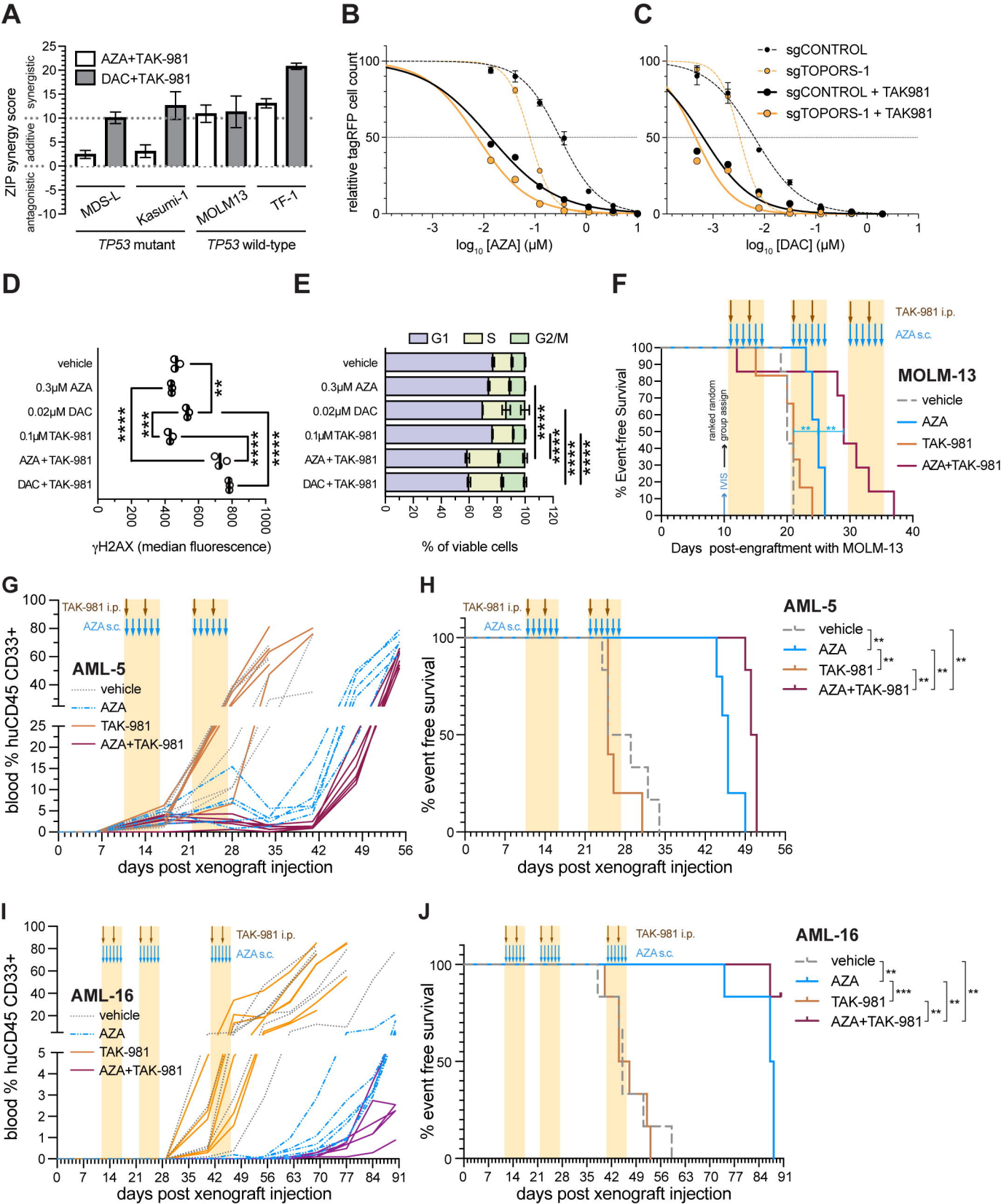


Figure 9